Title
STUDY OF THE REGENERATIVE EXTRACTOR OF THE BERKELEY 184-INCH-SYNCHROCYCLOTRON

Author
Paul, Arthur C.

Publication Date
1968-04-24

University of California

Ernest O. Lawrence Radiation Laboratory

STUDY OF THE REGENERATIVE EXTRACTOR OF THE BERKELEY 184-INCH SYNCHROCYCLOTRON

Arthur C. Paul

April 24, 1968

Berkeley, California

DISCLAIMER

UCRL-18211
UC-28 Particle Accel.
and High Volt. Mach.
TID-4500 (52nd Ed.)

UNIVERSITY OF CALIFORNIA

Lawrence Radiation Laboratory
Berkeley, California

AEC Contract No. W-7405-eng-48

STUDY OF THE REGENERATIVE EXTRACTOR OF THE BERKELEY 184-INCH-SYNCHROCYCLOTRON

Arthur C. Paul

April 24, 1968

Printed in the United States of America
Available from
Clearinghouse for Federal Scientific and Technical Information
National Bureau of Standards, U. S. Department of Commerce
Springfield, Virginia 22151
Price: Printed Copy $3.00; Microfiche $0.65

Contents

Abstract v

I. Introduction 1

II. General Features of the 184-Inch Extraction System 3

III. General Features of Regenerative Extraction 12

IV. Betatron Phase Space 12

V. Calculation of the Extraction Efficiency 19

VI. The Vertical Distribution 26

VII. The Radial Distribution 26

VIII. External Beam Acceptance Factors 30

IX. Orbit Calculations. 30

X. Results 44

XI. Effect of Low Energy Penetration into the Regenerator . . . 48

UCRL-18211

Study of the Regenerative Extractor of the Berkeley 184-Inch Synchrocyclotron

Arthur C. Paul

April 24, 1968

ABSTRACT

The behavior of the regenerative extractor of the Berkeley 184-Inch cyclotron has been studied by separating the properties of the incident beam from the properties of the regenerator. This was accomplished by considering the extraction efficiency as the product of two quantities, the differential extraction efficiency determined by the magnetic field perturbations, and the phase space density determined by the quality of the beam incident upon the regenerator.

The calculations are based on the study of some 1500 particles representing a sampling over energy (radial amplitude), radial betatron phase (azimuth of maximum radial amplitude), vertical betatron amplitude, and vertical betatron phase.

The particles are started inside the stable region of the radial betatron phase space and accelerated through at least one complete precessional oscillation (40-100 revolutions) before gaining sufficient energy to cross the separatrix of the phase space diagram and begin regeneration. During this precessional revolution they sample entry into the regenerator without extraction. Once outside the stable region, regeneration sets in with the cessation of the radial betatron precession.

Five distinct mechanisms of particle loss have been found associated with the beam extraction system, Fig. 1: Mode 1--axial growth and subsequent vertical loss of the low energy beam penetrating into the regenerator field but not deep enough for the onset of regeneration; Mode 2--resumption of radial precession during regeneration, resulting in vertical loss of the beam or exit from the magnetic field at the wrong azimuth; Mode 3--successfully regenerated beam failing to pass through the magnetic channel aperture; Mode 4--vertical loss of the successfully regenerated beam at $\nu_z = 1/2$ by overfocusing in the last several turns in the rapidly falling fringing field of the cyclotron (peeler field); and Mode 5--mismatch between the phase space acceptance of the external beam and the emittance of the beam leaving the cyclotron. The relative importance of the various modes of loss depends on the betatron oscillation amplitudes and, hence, is determined by the quality of internal beam incident on the regenerator.

The extraction efficiency for the 184-inch cyclotron is found to be dominated by the vertical beam growth at $\nu_z = 1/2$ and the radial width of the magnetic channel. The results of the computer study based on the measured magnetic field data of the 184-inch cyclotron have been verified by actual measurements carried out at the cyclotron. Favorable comparison has been obtained between predicted and measured values, including: 1) extraction efficiency, 2) dependence of extraction efficiency on the radial and vertical betatron oscillation amplitudes, 3) external beam energy;

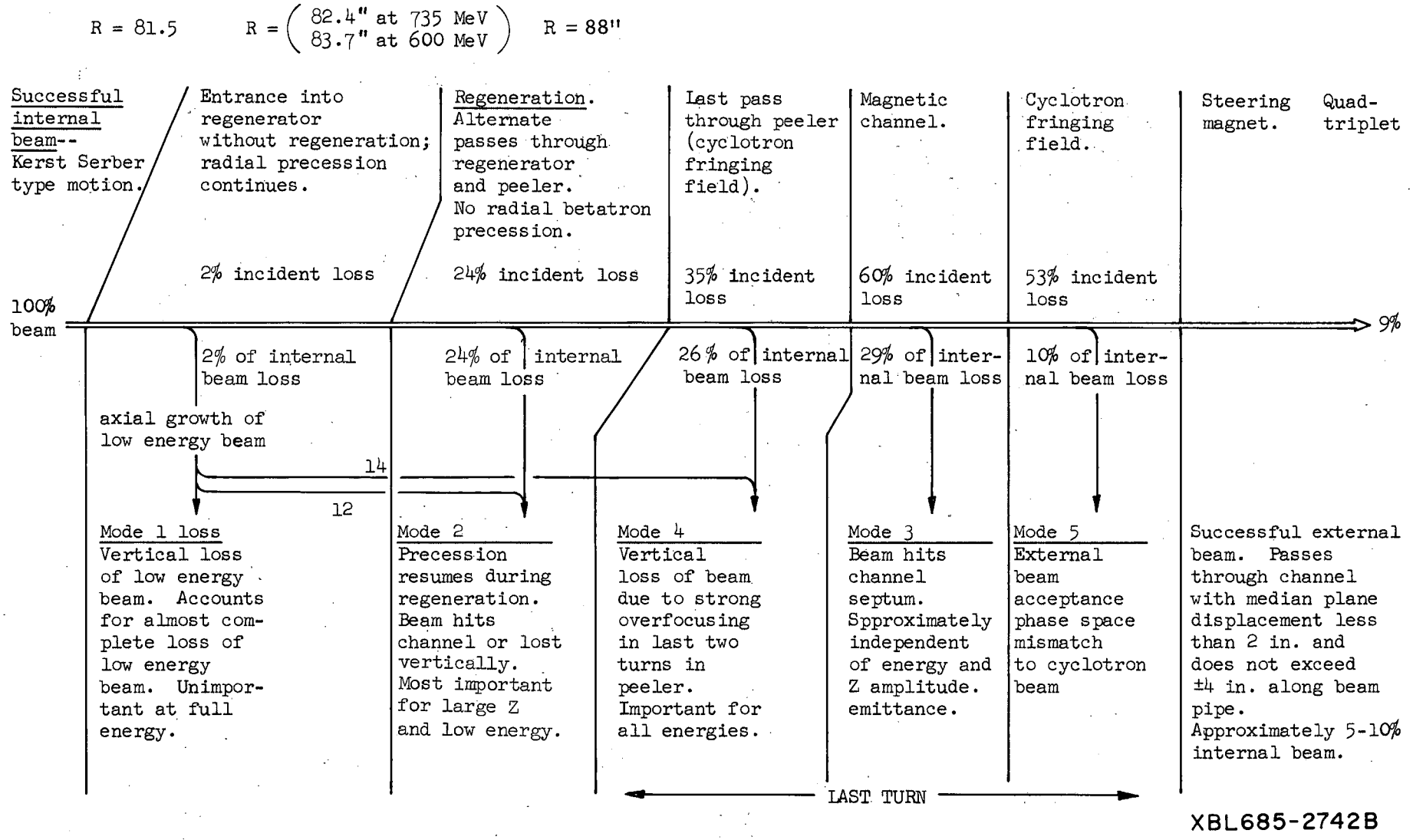

Fig. 1. Loss mechanisms of the extraction system for the 184-inch synchrocyclotron. The percentage of internal beam lost by each mode is indicated for the measured magnetic field and observed particle distribution. Also given is percentage of incident beam loss by each mode.

UCRL-18211

4) external beam energy distribution, and 5) spacial beam profiles. The calculated extraction efficiency of 9% compares favorably with present machine operation.

I. INTRODUCTION

Widespread use has been made of regenerative extraction for the removal of internal beams from synchrocyclotrons. Magnetic field perturbations close to the final radius of the cyclotron build up the radial oscillation amplitude of the internal beam sufficiently to allow particles to emerge from the magnetic field of the cyclotron. Systems employing either linear[1,2] or non-linear[3,4] fields have been studied and applied to almost all synchrocyclotrons[5-9] around the world. In practice, almost all the machines exhibit an extraction efficiency of only a few percent, even though they differ greatly in size, energy, and configuration. The need for higher intensity external beams for the performance of difficult experiments has inspired attempts to improve the synchrocyclotron output. The strong possibility of a large increase in the internal current of synchrocyclotrons by reduction of the space charge blowup near the source,[10] combined with the requirement of large external beam intensities and the near-maximum internal radiation activation limit of present machines, makes very desirable a better understanding of the poor extraction efficiency and its subsequent improvement.

---

1 K. J. LeCouteur, The Regenerative Deflector for Synchrocyclotrons, Proc. Phys. Soc. (London) B64, 1073 (1951).

2 A. V. Crewe, K. J. LeCouteur, Extraction of Beam From the Liverpool Synchrocyclotron, Proc. Roy. Soc. (London) A232, 242 (1955).

3 K. J. LeCouteur, S. Lipton, Non-Linear Regenerative Extraction of Sychrocyclotron Beams, Phil. Mag. 46, 265 (1955).

4 K. J. LeCouteur, Perturbations in the Magnetic Deflector for Synchrocyclotrons, Proc. Phys. Soc. B64, 25 (1952).

5 S.Kullander et al., (Uppsala 185 MeV Cyclotron, 1% extraction efficiency) IEEE Transactions NS-12, 106 (1966).

6 Ken Crowe (Berkeley 750 MeV Cyclotron, 5% extraction efficiency) William and Mary Conference on Cyclotron Improvement, 108 (1964).

7 A. V. Crewe, K. J. LeCouteur (Liverpool 380 MeV Cyclotron, 3% extraction efficiency) Rev. Sci. Instr. 26, 725 (1955).

8 A.V. Crewe, V. E. Kruse (Chicago 450 MeV Cyclotron 3% extraction efficiency) Rev. Sci. Instr. 27, 5 (1956).

9 MSC Staff Proposal for the Improvement of the 600 MeV Synchrocyclotron, CERN (1967), private communication (5% extraction efficiency).

10 K. R. MacKenzie, Synchrocyclotron Conversion, IEEE Transactions NS-13, 220 (1966).

Kim[11,12] has suggested possible improvements for synchrocyclotron regenerative extractors. One possible improvement here lies in the energy compression of the beam entering the regenerator by a time-varying field harmonic. This appears to give a reasonable improvement in extraction efficiency for sufficiently large radial oscillation amplitudes provided it does not force the beam through the Walkinshaw resonance, where $\nu_r = 2\nu_z$. However, the calculations presented here show that the improvement for the observed particle distribution of the 184-inch cyclotron would be very small. More important is the loss incurred by the vertical amplitude growth at the end of regeneration.[13] Here, the deep penetration into the peeler field on the last two revolutions produces too strong a vertical focusing force to be compensated by the regenerator. The vertical motion is driven into resonance at $\nu_z = 1/2$ in the same manner as the radial motion is driven by regeneration into resonance at $\nu_r = 1$.

The calculation of extraction efficiency is based on the study of particles accelerated through at least one radial precessional motion into regenerative action. A representative sampling is made in energy (radial amplitude), radial betatron phase (azimuth of maximum radial amplitude), vertical betatron amplitude and phase. The experimentally measured phase space density is used. The calculated extraction efficiency and energy distributions in the external beam compare with the measured values to within the experimental uncertainties. The calculated beam profile compares favorably with that determined from beam photographs.

The calculations assume that: 1) the integration of the exact differential equations of motion using only the first-order terms in a Taylor series expansion of the magnetic field about the median plane adequately describe the particle motion; 2) the magnetic field changes made since the last field measurements[14] produce no significant alterations in the operation of the regenerator; 3) the details of the calculations do not depend on the rate of energy gain of the particles provided that this rate is sufficiently small; 4) the sampling of a single radial betatron precession before regeneration begins is sufficient to sample

---

[11] D. J. Clark, Hogil Kim, K. R. MacKenzie, J. Vale, Modification Studies for the 184-Inch Cyclotron, NS-13, 235 (1966).

[12] Hogil Kim, Regenerative Beam Extraction, IEEE Transactions NS-13, 58 (1966).

[13] A. C. Paul, Lawrence Radiation Laboratory Report UCID-3142 (1968).

[14] The last complete field measurements were made in June 1957. Since that time a pancake has been removed from the lower main coil and the main and auxiliary coil excitations have been increased. The net result has been to increase the magnetic field by about 100 G. Also, the regenerator has been physically moved 1/4 in. outward in radius; and the magnetic channel has been physically moved 13/16 in. inward in radius.

particle behavior inside the extraction radius; 5) sampling over the vertical phase space is represented by vertically conjugate pairs of particles;[15] and 6) the synchrotron oscillations can be neglected since they are small compared with the betatron oscillations.

II. GENERAL FEATURES OF THE 184-INCH EXTRACTION SYSTEM

The regenerative extraction system of the 184-inch cyclotron was installed in 1957 and reported by Stubbins et al.[16,17,18] The physical features are typical of a non-linear regenerator using the fringing field of the cyclotron as a peeler. The layout is shown in Fig. 2. The magnetic field perturbations of the regenerator begin at 81.5 in. and extend over a 10-deg azimuthal interval centered at 116 deg, Figs. 3 and 4. The regenerator reaches a peak perturbation of 6 kG at 88 in. and falls to zero at 91 in. On the last revolution particles pass behind the regenerator at 91 in. and enter the magnetic channel. The channel has a peak gradient of 1400 G/in. in the reverse direction to the cyclotron fringing field. The channel shown in Fig. 5 is horizontally focusing and does not deflect the central (paraxial) ray. The radial field used in the orbit calculations is given in Table 1 and corresponds to a main coil excitation of 0.48663 V (1530 A) and an auxiliary coil excitation of 0.4698 V (2660 A).[19] The field perturbations produced by the regenerator and magnetic channel are given in Tables 2 and 3.[20]

---

[15] By a vertically conjugate pair of particles, I mean one of maximum amplitude z_m with $P_z = 0$ and the other with $z = 0$ and maximum momentum P_{z_m} corresponding to the value of z_m; i.e., $(z,0)$ and $(0,P_z)$, Fig. 11.

[16] W. F. Stubbins, E. L. Kelly, J. T. Vale, K. Crowe, Bull. Amer. Phys. Soc. II.2, 382 (1957).

[17] W. F. Stubbins, Lawrence Radiation Laboratory Report UCRL-3476 (1957).

[18] W. F. Stubbins, Rev. Sci. Instr. 29 (1958).

[19] The auxiliary coil shunt calibration of June 12, 1957, gives 5.67 A/mV and the main coil shunt calibration 3.133 A/mV, while the present shunt calibrations measured Feb. 23, 1968, gives 5.4313 A/mV and 3.0024 A/mV respectively.

[20] The basic data is taken from magnetic field measurements group Log book 282 (6-21-57), Runs 205-228. The channel perturbations are taken from this same book while the regenerator perturbations are based on analyzed data of Runs 698-712.

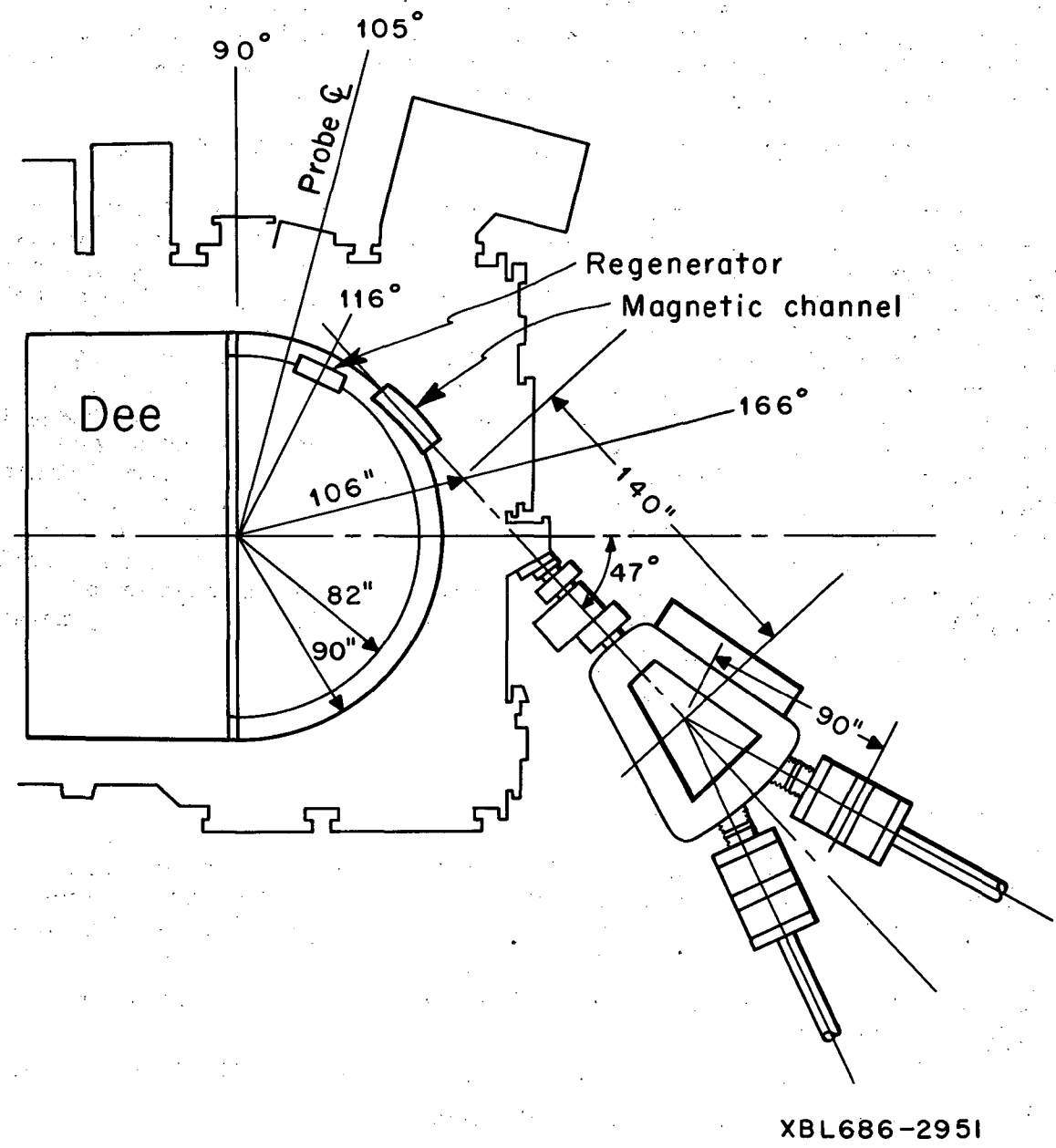

Fig. 2. Plan view of cyclotron and first two external beam magnets.

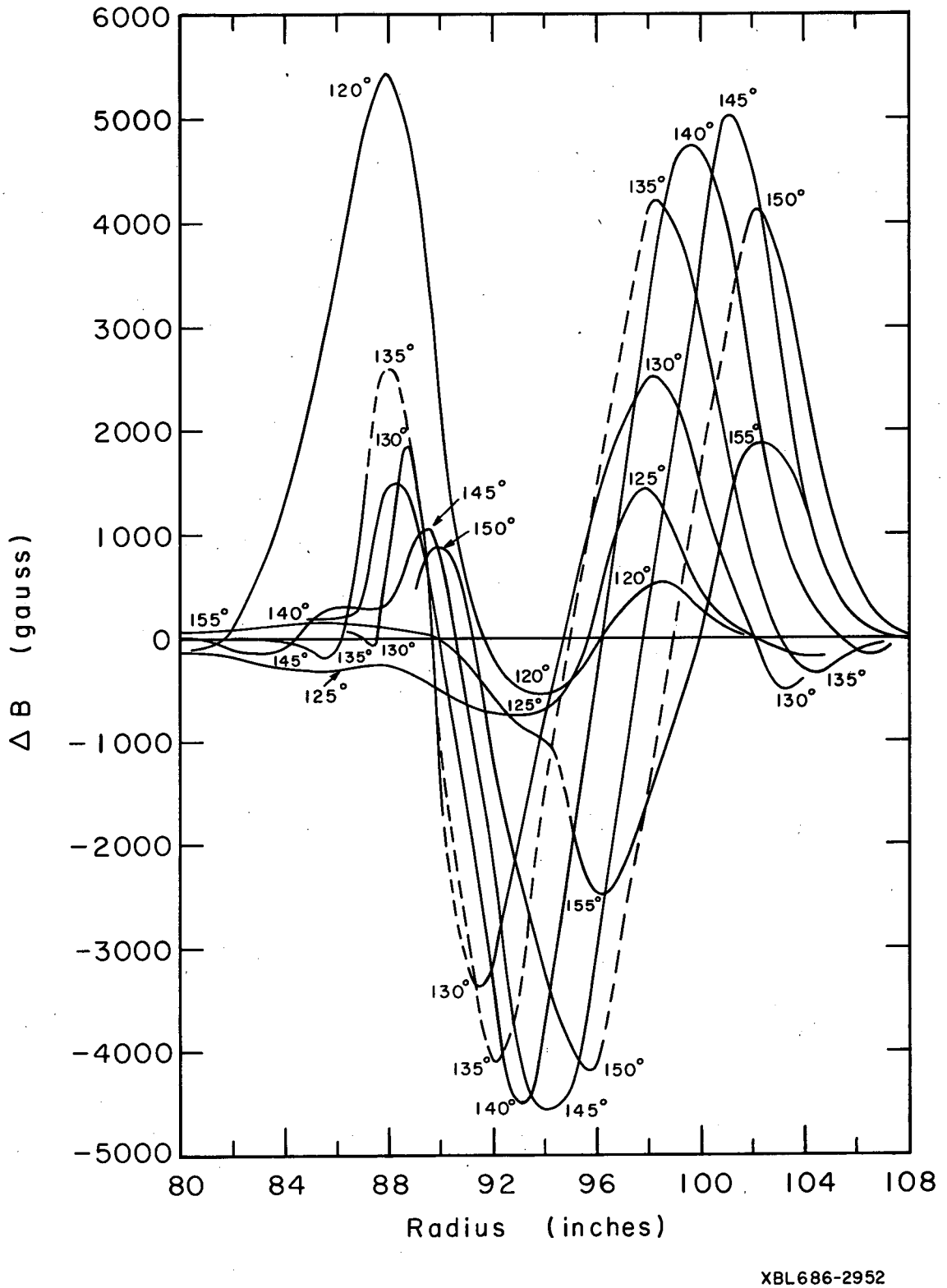

Fig. 3. Magnetic field perturbations for 184-inch cyclotron.

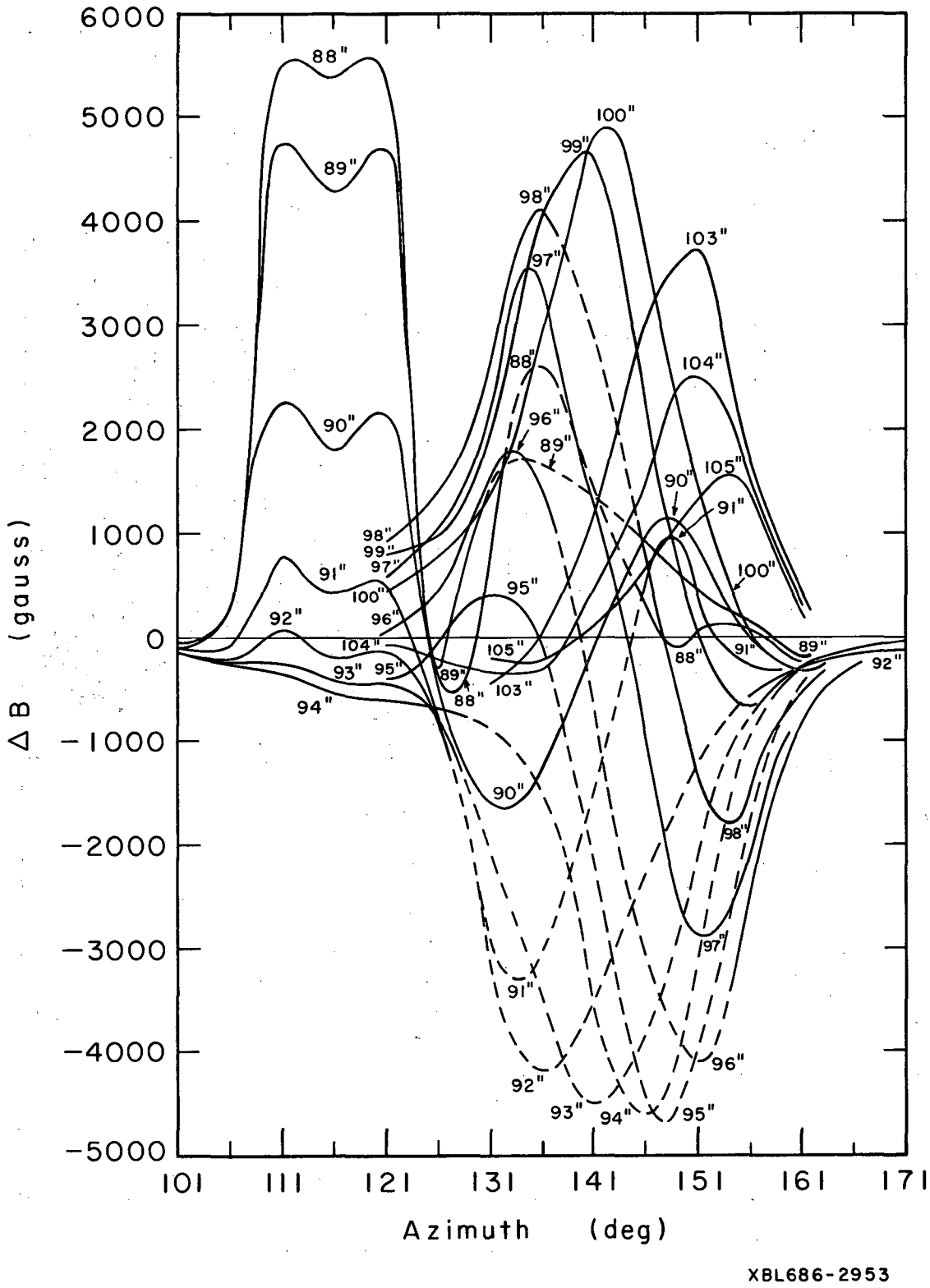

Fig. 4. Magnetic field perturbations of regenerator and magnetic channel.

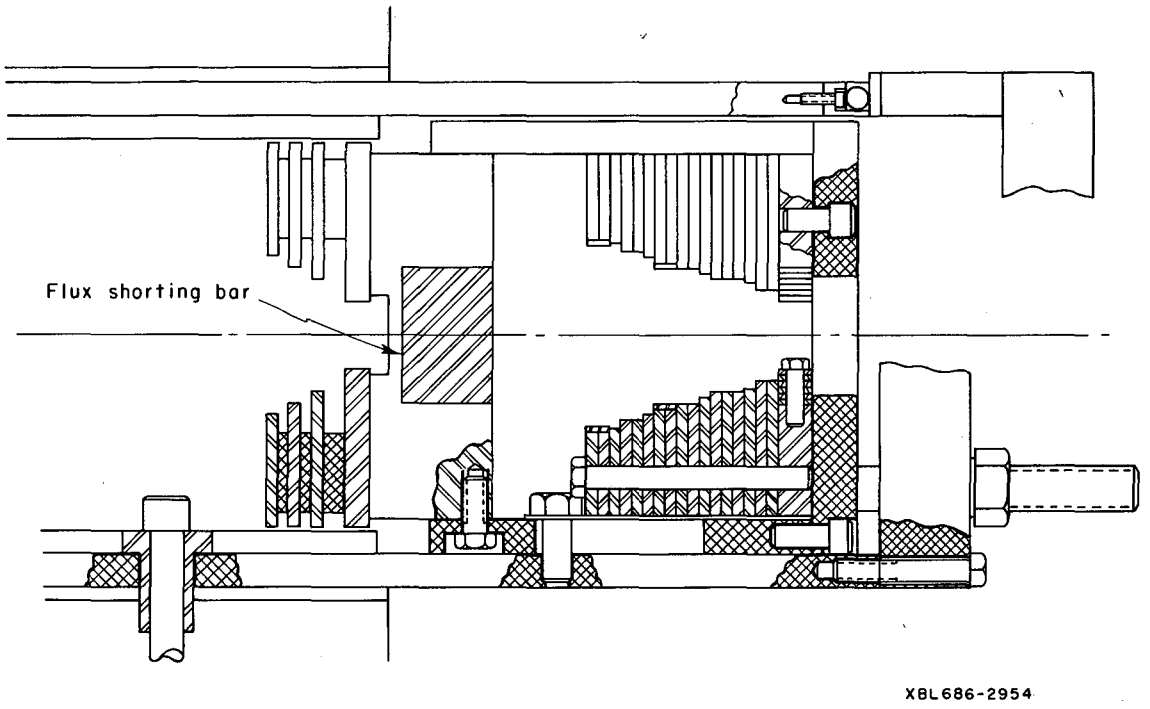

Fig. 5. Cross section of magnetic channel, showing flux shorting bar.

Table 1. The radial magnetic field of the 184-inch cyclotron and related parameters. Index $\equiv -$ dB R/dR B, $\gamma \equiv (1-\beta^2)^{-1/2}$, $E = E_0 \gamma$, $F \equiv eB/2\pi mc$, $\nu_r \equiv (1-n)^{1/2}$, and $\nu_z = \sqrt{n}$.

R (in.)	B (G)	N = field index	γ	E (MeV)	F (MHz)	ν_z	ν_R
1	23347	.00090	1.0002	.2	35.64	.0300	.9996
2	23327	.00169	1.0007	.7	35.59	.0412	.9992
3	23306	.00277	1.0016	1.5	35.53	.0527	.9986
4	23284	.00397	1.0029	2.7	35.45	.0630	.9980
5	23261	.00499	1.0044	4.2	35.36	.0707	.9975
6	23238	.00567	1.0064	6.0	35.25	.0753	.9972
7	23217	.00603	1.0087	8.1	35.14	.0776	.9970
8	23198	.00623	1.0113	10.6	35.02	.0789	.9969
9	23181	.00654	1.0142	13.4	34.89	.0809	.9967
10	23164	.00716	1.0175	16.4	34.76	.0846	.9964
11	23147	.00806	1.0211	19.8	34.61	.0898	.9960
12	23130	.00904	1.0251	23.5	34.45	.0951	.9955
13	23112	.01012	1.0293	27.5	34.28	.1006	.9949
14	23094	.01132	1.0339	31.8	34.10	.1064	.9943
15	23075	.01241	1.0387	36.3	33.92	.1114	.9938
16	23056	.01315	1.0439	41.1	33.72	.1147	.9934
17	23037	.01336	1.0493	46.3	33.52	.1156	.9933
18	23020	.01296	1.0550	51.6	33.31	.1138	.9935
19	23004	.01234	1.0611	57.3	33.10	.1111	.9938
20	22990	.01199	1.0674	63.2	32.88	.1095	.9940
21	22977	.01185	1.0739	69.4	32.66	.1089	.9941
22	22964	.01177	1.0808	75.8	32.44	.1085	.9941
23	22952	.01195	1.0879	82.5	32.21	.1093	.9940
24	22940	.01260	1.0953	89.4	31.98	.1123	.9937
25	22928	.01361	1.1029	96.6	31.74	.1166	.9932
26	22915	.01482	1.1108	103.9	31.50	.1217	.9926
27	22902	.01596	1.1189	111.5	31.25	.1263	.9920
28	22888	.01676	1.1272	119.3	31.00	.1295	.9916
29	22874	.01769	1.1357	127.3	30.75	.1330	.9911
30	22860	.01922	1.1445	135.5	30.50	.1386	.9903
31	22845	.02051	1.1534	143.9	30.24	.1432	.9897
32	22830	.02065	1.1626	152.5	29.98	.1437	.9896
33	22816	.02023	1.1719	161.3	29.72	.1422	.9898
34	22802	.02004	1.1815	170.3	29.46	.1416	.9899
35	22789	.01997	1.1912	179.4	29.21	.1413	.9900
36	22776	.01978	1.2012	188.8	28.95	.1407	.9901
37	22764	.01951	1.2113	198.3	28.69	.1397	.9902
38	22752	.01917	1.2216	207.9	28.43	.1384	.9904
39	22741	.01883	1.2321	217.8	28.18	.1372	.9905
40	22730	.01861	1.2428	227.8	27.92	.1364	.9907
41	22720	.01885	1.2536	238.0	27.67	.1373	.9905
42	22709	.01983	1.2646	248.3	27.42	.1408	.9900
43	22698	.02091	1.2757	258.7	27.16	.1446	.9895
44	22687	.02139	1.2870	269.3	26.91	.1462	.9892
45	22676	.02177	1.2984	280.0	26.66	.1475	.9891
46	22665	.02267	1.3100	290.8	26.42	.1506	.9886
47	22654	.02386	1.3216	301.8	26.17	.1545	.9880
48	22642	.02499	1.3334	312.8	25.92	.1581	.9874
49	22630	.02603	1.3454	324.0	25.68	.1613	.9869
50	22618	.02691	1.3574	335.3	25.44	.1640	.9865

Table 1. (contd.)

R (in.)	B (G)	N = field index	γ	E (MeV)	F (MHz)	ν_z	ν_R
51	22606	.02720	1.3695	346.7	25.20	.1649	.9863
52	22594	.02655	1.3818	358.2	24.96	.1629	.9866
53	22583	.02573	1.3941	369.8	24.73	.1604	.9870
54	22572	.02564	1.4066	381.5	24.50	.1601	.9871
55	22561	.02563	1.4193	393.4	24.27	.1601	.9871
56	22551	.02485	1.4320	405.3	24.04	.1577	.9875
57	22541	.02505	1.4448	417.3	23.82	.1583	.9874
58	22531	.02773	1.4577	429.4	23.60	.1665	.9860
59	22520	.02832	1.4707	441.6	23.38	.1683	.9857
60	22510	.02260	1.4838	453.9	23.16	.1503	.9886
61	22503	.01563	1.4971	466.4	22.95	.1250	.9922
62	22498	.01327	1.5105	479.0	22.74	.1152	.9933
63	22493	.01496	1.5241	491.7	22.53	.1223	.9925
64	22487	.01905	1.5376	504.4	22.33	.1380	.9904
65	22479	.02460	1.5513	517.2	22.12	.1568	.9876
66	22470	.03020	1.5649	530.0	21.92	.1738	.9848
67	22459	.03466	1.5785	542.7	21.72	.1862	.9825
68	22447	.03716	1.5921	555.5	21.53	.1928	.9812
69	22435	.03727	1.6058	568.3	21.33	.1931	.9812
70	22423	.03513	1.6195	581.3	21.14	.1874	.9823
71	22412	.03167	1.6334	594.3	20.95	.1780	.9840
72	22403	.02810	1.6474	607.4	20.76	.1676	.9858
73	22395	.02574	1.6615	620.6	20.58	.1604	.9870
74	22387	.02535	1.6757	633.9	20.40	.1592	.9872
75	22379	.02671	1.6899	647.3	20.22	.1634	.9866
76	22371	.02884	1.7042	660.7	20.04	.1698	.9855
77	22362	.02965	1.7185	674.1	19.87	.1722	.9851
78	22354	.02906	1.7328	687.5	19.70	.1705	.9854
79	22346	.02716	1.7472	701.1	19.53	.1648	.9863
80	22338	.03037	1.7617	714.7	19.36	.1743	.9847
81	22326	.06330	1.7760	728.1	19.19	.2516	.9678
82	22298	.15350	1.7895	740.7	19.02	.3918	.9201
83	22236	.32496	1.8010	751.5	18.85	.5701	.8216
84	22116	.59454	1.8093	759.3	18.66	.7711	.6368
85	21916	.95608	1.8127	762.5	18.46	.9778	.2096
86	21618	1.39927	1.8102	760.1	18.23	1.1829	-.3993
87	21209	1.91017	1.8008	751.3	17.98	1.3821	-.9102
88	20685	2.47363	1.7840	735.6	17.70	1.5728	-1.4736
89	20043	3.14499	1.7596	712.6	17.39	1.7734	-2.1450
90	19265	3.97455	1.7264	681.5	17.04	1.9936	-2.9745
91	18347	4.84340	1.6841	641.8	16.63	2.2008	-3.8434
92	17327	5.59560	1.6352	596.0	16.18	2.3655	-4.5956
93	16256	6.18222	1.5829	546.9	15.68	2.4864	-5.1822
94	15180	6.58749	1.5301	497.4	15.15	2.5666	-5.5875
95	14136	6.88244	1.4792	449.6	14.59	2.6234	-5.8824
96	13133	7.19028	1.4308	404.1	14.01	2.6815	-6.1903
97	12169	7.50974	1.3849	361.1	13.42	2.7404	-6.5097
98	11250	7.79896	1.3419	320.8	12.80	2.7927	-6.7990
99	10380	8.06175	1.3021	283.5	12.17	2.8393	-7.0618
100	9560	8.30087	1.2657	249.3	11.53	2.8811	-7.3009

Table 2. Regenerator perturbations, in gauss.

R (in.)	Azimuth 101°	106°	111°	116°	121°	126°	131°	136°	141°	146°	151°	156°	161°	166°	171°
71	-32	-21	50	-2	-60	-110	-27	-65	29	28	87	85	92	79	-66
72	-3	-8	58	-1	-56	-115	-23	-76	24	28	89	81	97	92	-65
73	25	-4	66	7	-50	-120	-17	-78	14	22	86	71	99	102	-65
74	35	-9	74	16	-45	-118	4	-60	8	7	79	55	102	115	-65
75	41	-20	84	23	-40	-109	38	-27	23	9	66	37	101	124	-63
76	40	-33	90	21	-37	-97	68	18	49	21	54	13	99	134	-65
77	35	-51	80	8	-56	-92	88	40	65	40	47	-14	94	143	-65
78	43	-77	71	4	-63	-104	102	34	66	54	54	-40	85	144	-71
79	49	-86	86	14	-54	-106	97	3	47	39	71	-46	74	136	-65
80	45	-99	81	1	-102	-125	81	-36	14	10	76	-27	51	114	-60
81	41	-86	64	2	-106	-150	70	-59	-23	-48	55	16	19	87	-58
82	32	-65	219	233	36	-174	88	-28	-51	104	21	65	-18	40	-59
83	14	-9	672	813	481	-217	102	31	28	-139	-17	108	-56	-12	-70
84	1	56	1484	1741	1282	-277	103	15	164	-74	-52	142	-96	-64	-81
85	-10	120	2632	2962	2427	-313	104	-83	217	94	-50	165	-136	-108	-88
86	-15	174	3845	4178	3635	-302	66	-101	218	220	1	185	-169	-132	-88
87	-15	222	4967	5387	4796	-281	4	1056	395	217	54	203	-197	-144	-83
88	-30	241	5838	5979	5705	-283	829	0	1396	289	143	227	-239	-149	-79
89	-68	192	4741	4300	4672	-367	1523	0	0	910	429	173	-256	-156	-86
90	-101	58	2340	1829	2210	-527	-1509	0	0	0	849	2	-293	-169	-100
91	-130	-104	785	427	582	-664	0	0	0	0	0	-282	-302	-167	-104
92	-147	-207	43	-203	-163	-702	0	0	0	0	0	-589	-307	-161	-101
93	-149	-250	-247	-444	-474	-726	0	0	0	0	0	-798	-288	-134	-81
94	-151	-257	-365	-524	-601	-684	0	0	0	0	0	-913	-280	-122	-81

Table 3. Magnetic channel perturbations, in gauss.

R (in.)	Azimuth														
	101°	106°	111°	116°	121°	126°	131°	136°	141°	146°	151°	156°	161°	166°	171°
88	0	0	0	0	0	0	0	2600	0	0	0	0	0	0	0
89	0	0	0	0	0	0	0	1650	1350	0	0	0	0	0	0
90	0	0	0	0	0	0	0	-1250	150	950	0	0	0	0	0
91	0	0	0	0	0	0	-3000	-2750	-1500	650	450	0	0	0	0
92	0	0	0	0	0	0	-3200	-4200	-3500	-2250	-1250	0	0	0	0
93	0	0	0	0	0	0	-2000	-3500	-4500	-4000	-2250	0	0	0	0
94	0	0	0	0	0	0	-900	-1400	-3750	-4600	-3200	0	0	0	0
95	0	0	0	0	400	-400	400	0	-2100	-4650	-3900	-1750	-500	-113	0
96	0	0	0	0	0	500	1500	1400	-400	-2950	-4200	-2500	-850	-122	0
97	0	0	0	0	600	1100	2100	3500	1250	-1250	-2800	-2100	-300	-133	0
98	0	0	0	0	1000	1400	2500	4200	2950	400	-1400	-1500	-500	-112	0
99	0	0	0	0	800	1000	2250	4000	4650	2150	0	-750	-100	-108	0
100	0	0	0	0	500	800	1400	3000	4750	3800	1400	0	-50	-114	0
101	0	0	0	0	200	300	500	1750	4050	5000	2800	1000	300	-103	0
102	0	0	0	0	50	50	50	750	2500	4500	4200	1800	400	0	-0
103	0	0	0	0	0	-50	-500	0	1250	3000	3750	1750	400	0	0
104	0	0	0	0	-50	-200	-350	-300	550	1500	2500	1500	300	0	0
105	0	0	0	0	-75	-100	-200	-250	150	500	1350	1350	200	0	0
106	0	0	0	0	0	0	0	0	0	0	550	500	0	0	0
107	0	0	0	0	0	0	0	0	0	0	200	150	0	0	0
108	0	0	0	0	0	0	0	0	0	0	0	0	0	0	0

III. GENERAL FEATURES OF REGENERATIVE EXTRACTION

Inside the radius of the regenerator perturbations the particles execute oscillations determined by the azimuthally independent weak focusing field. Regeneration begins when the precession of the maximum radial displacement is stopped. Then the radial amplitude increases exponentially by the alternate action of the regenerator perturbations and the influence of the peeler field. The radius at which this begins depends on the particle energy and ranges between 82.0 in. for full energy beam and 83.2 in. for a 700-MeV energy beam. Loss of particles by axial blowup must be eliminated for efficient removal of the beam from the cyclotron. At present 25-30% of the internal beam is lost vertically before leaving the face free plate of the cyclotron. This beam loss is brought about by the peeler's driving the vertical motion at $\nu_z = 1/2$.

Consider particles of small radial oscillation amplitude being slowly accelerated into the regenerative field, Fig. 6. After regeneration begins, particles at the center of the regenerator (116 deg) are deflected inward by regenerator perturbations of such strength that they cross the equilibrium orbit at about 168 deg azimuth. The particles so deflected begin a radial oscillation of larger amplitude passing through a node close to zero degrees azimuth. They now pass further into the peeler (farther out in radius) and experience a weaker magnetic field than before; this causes them to reach the azimuth of the regenerator at still a larger radius and experience an even stronger regenerator field which drives them even more strongly inward. The regenerator builds the amplitude up to a maximum of 9 in. on the last turn with a turn separation of about 3 in. at the regenerator azimuth. The particles now have a radius of 91 in. at 116 deg azimuth and pass behind the regenerator and into the horizontally focusing magnetic channel.

Figure 6 shows three typical orbits. One orbit, Orbit A, is successfully regenerated into the external beam; Orbit B runs out of regenerator field and begins to precess; while Orbit C hits the channel Orbit B spends a large amount of time at large radius where the field index is large and, therefore, precesses rapidly. If it manages to encounter the regenerator at a favorable phase of this precessional motion, it may, on the next turn, emerge through the magnetic channel. However, more typically, it will precess until its vertical amplitude has increased sufficiently to be lost to the internal aperture of the cyclotron. Particles so lost are counted as a precessional loss even though they may be lost vertically.

IV. BETATRON PHASE SPACE

The 700 MeV static (non-accelerated) radial betatron phase space at 116 deg azimuth is shown in Fig. 7. Cyclotron units (cu) are used in these phase plots.[21] In this set of units the radius is measured in units

---

[21] Gordon and Welton, Oak Ridge National Laboratory Report ORNL-2765 (1959).

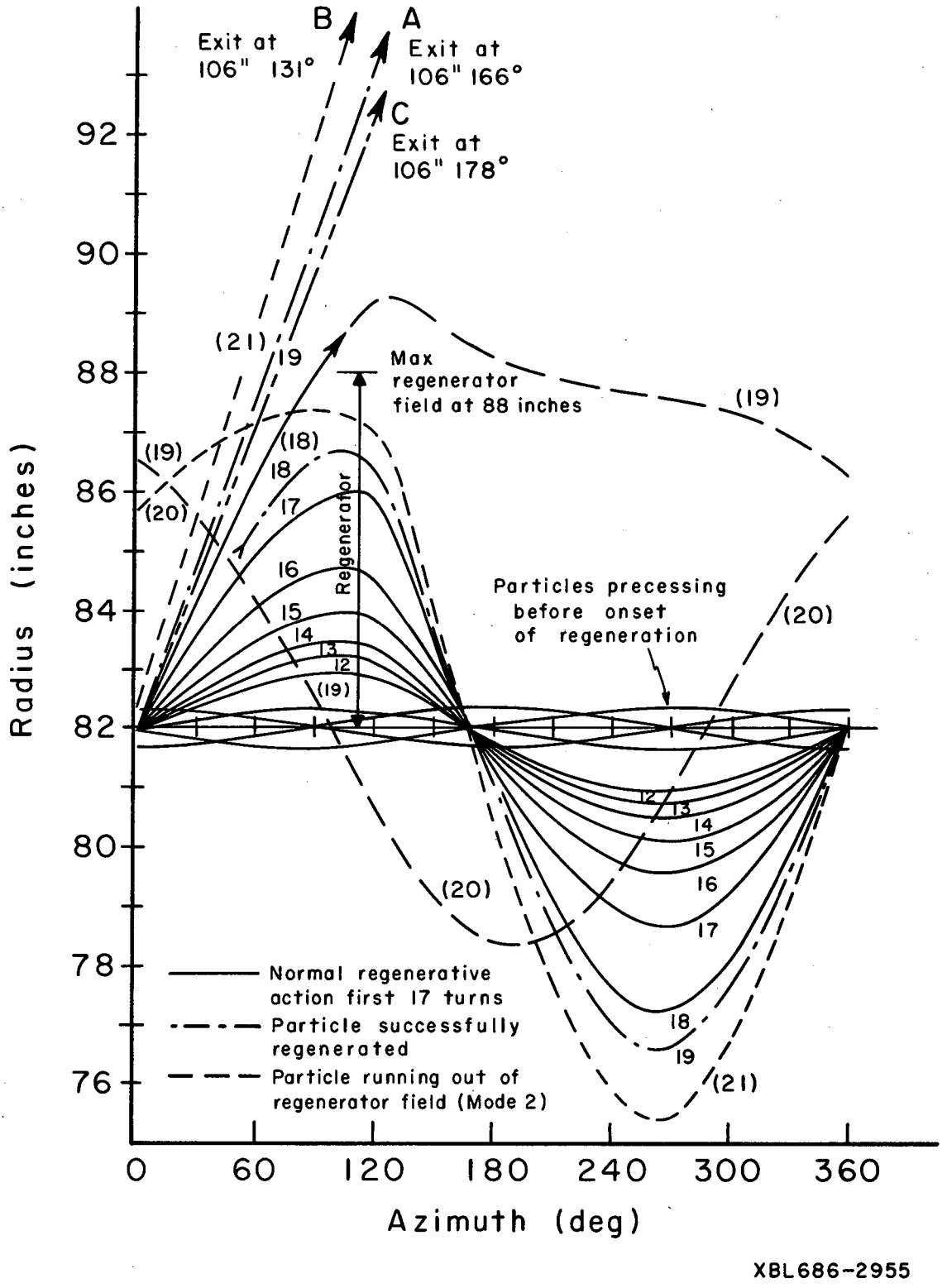

Fig. 6. Regenerative buildup of radial oscillation amplitude, showing normal particle (A) and precessional particle (B) ----.

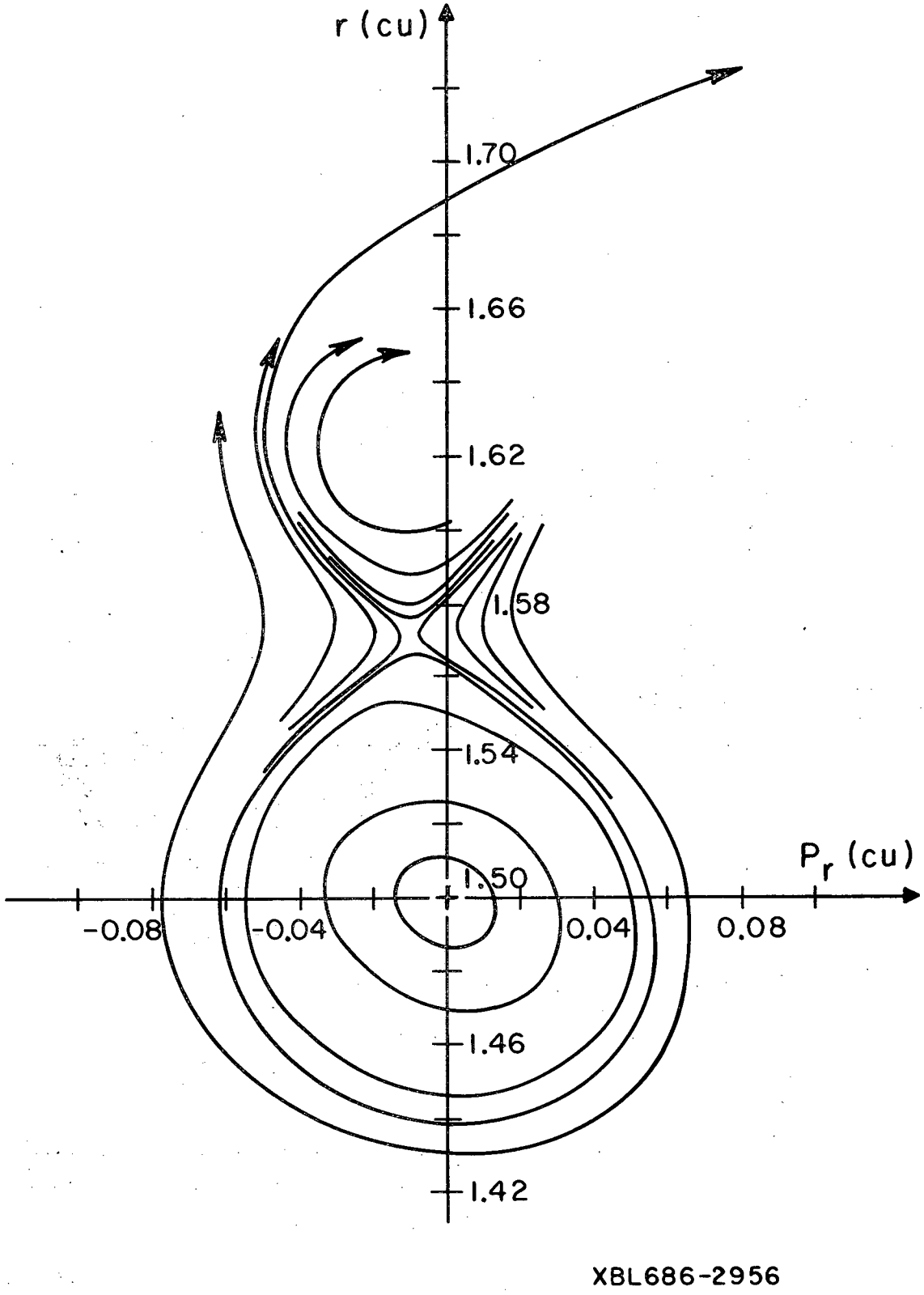

Fig. 7. Radial betatron phase plot of 184-inch cyclotron at 700 MeV; and 116° azimuth. Cyclotron units are used: 1 in. = 0.018951 cu.

of c/w_0, where w_0 is the rotational frequency of a particle of rest mass m_0 ($w_0 = eB/cm_0$) in a magnetic field B, and momentum is measured in units of m_0c (1 in. = 0.018951 cu for the 184-in. cyclotron). At 700 MeV the equilibrium orbit is located at 1.50,0. Particles executing radial betatron oscillations about the equilibrium orbit precess around the phase plot, forming closed orbits corresponding to different radial betatron oscillation amplitudes. The number of revolutions associated with the amplitude precession increases as the orbits get closer to the unstable fix point at 1.57, -0.01. An orbit headed directly at the unstable fix point would require an infinite number of revolutions to reach it. This limiting, closed orbit is called the separatrix of the phase diagram. Orbits of larger amplitude that lie outside the separatrix are not closed and are unstable in the sense that after a comparatively few revolutions the particles escape from the magnetic field. Orbits inside the separatrix are closed and stable since they remain inside for all time.

Accelerated particles of a given radial betatron amplitude started inside the separatrix have precessional motions relative to an equilibrium orbit which is gaining energy and, as a consequence, moves to larger radius with time. This radial motion of the equilibrium orbit by rf acceleration eventually carries a particle of given radial betatron oscillation amplitude across the separatrix. Figure 8 shows two particles of the same radial amplitude started at 700 MeV energy with different radial betatron phases. Particle A does not gain sufficient energy going from 1 to 2 to cross the separatrix. Its precessional motion is slowed down at 2 with sufficient energy gain there so that on the next precessional motion it crosses the separatrix and begins regeneration at point 3. Twenty-four revolutions are required to complete regeneration. Particle B, on the other hand, started at a different azimuth (radial phase) gains more energy in the first indicated precessional revolution so that it approaches closer to the unstable fix point. This slows down its precessional motion more than particle A so that it gains more energy here than particle A and on resumption of precession crosses the separatrix earlier in its next precessional revolution. Consequently, particle B begins regeneration at 3 farther from the unstable fix point and so requires fewer revolutions to complete regeneration; e.g., 16 turns.

The radial amplitude growth during regeneration is exponential so that the radius of the final turn is determined by the location of point 3, which is different for the two particles. The end of the regenerator tail of the phase diagram can be divided into three regions such that particle passage through a given region will determine if the particle 1) is successfully regenerated into the magnetic channel, 2) begins precession by running out of regenerator field, or 3) hits the magnetic channel. These three regions can be transformed back down the regeneration tail of the phase diagram as shown in Fig. 9(b). It can then be seen that there are bands of acceptable radial phase (starting azimuth) which will cause particles to enter the regeneration region such that they will be successfully regenerated into the external beam. The particles which fall into these bands are indicated by a (×). Particles which will not be successfully extracted are indicated by a (·). Since the betatron phase diagram is for a specific azimuth (e.g., 116 deg), the particles move discontinuously from point to point on the phase diagram. Nonetheless I have

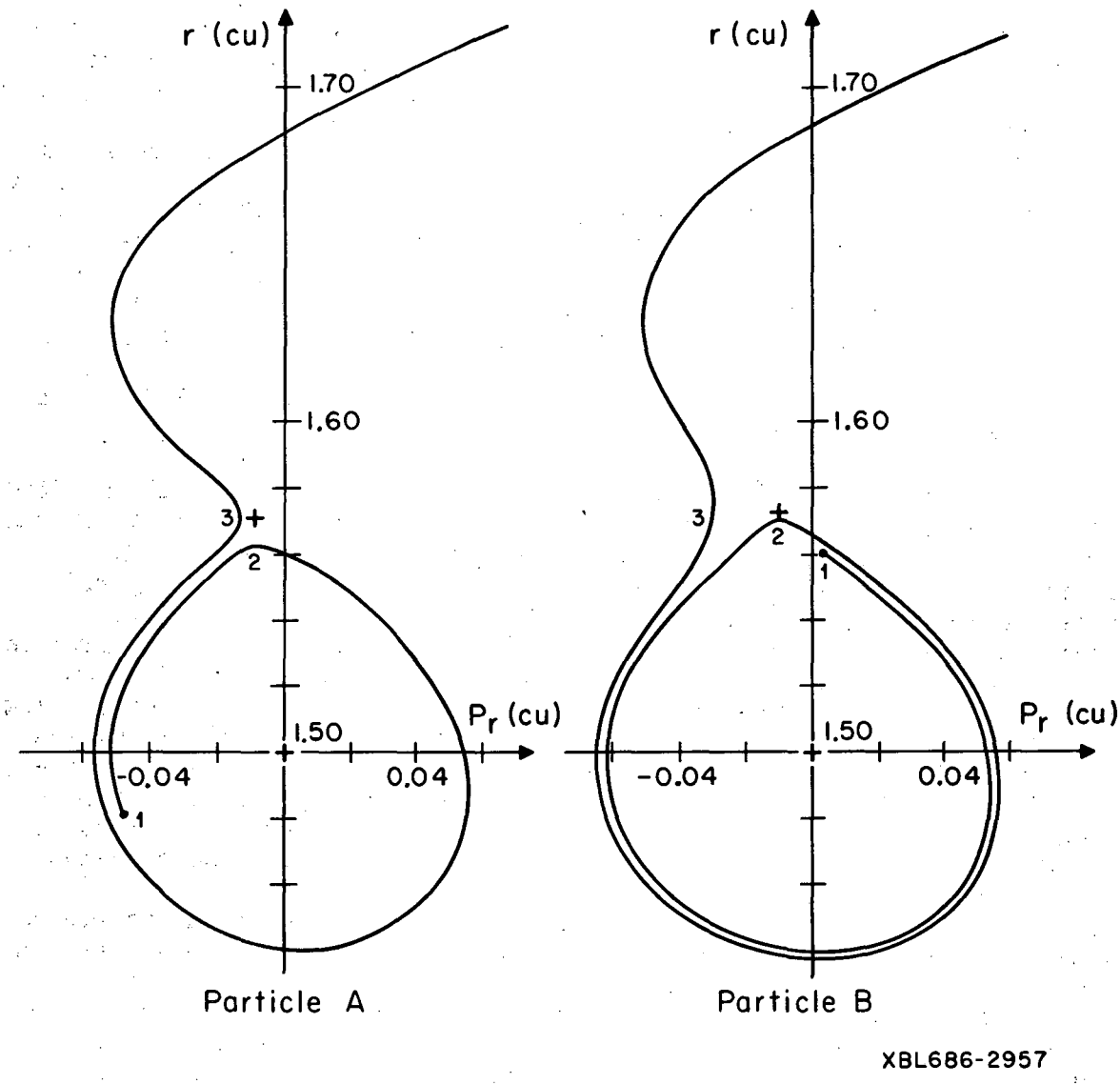

Fig. 8. Accelerated radial betatron phase motion for two particles of different starting azimuths.

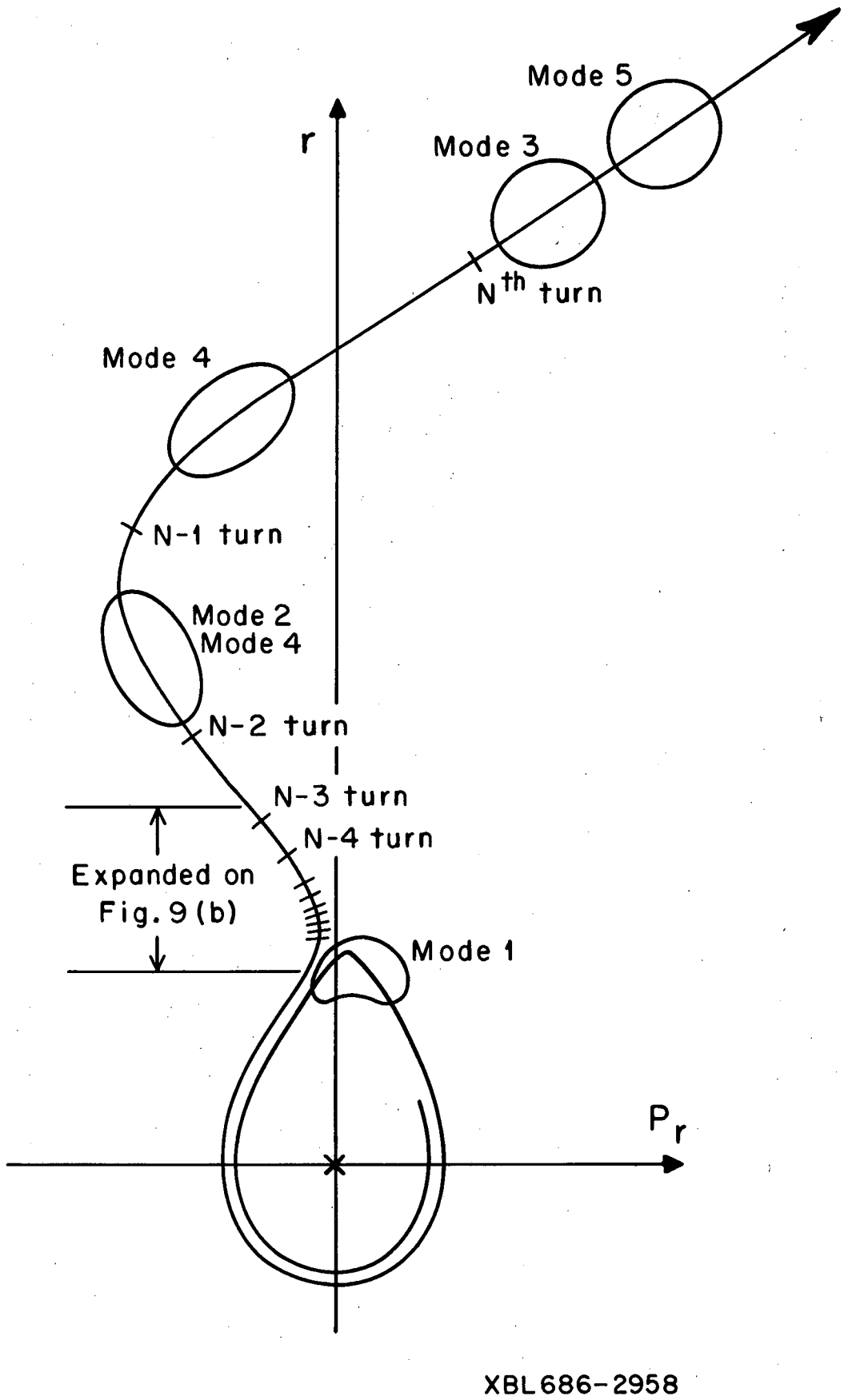

Fig. 9(a). Typical radial betatron phase plot showing location of successfully extracted particle and regions of loss. The particles are accelerated through the separatrix.

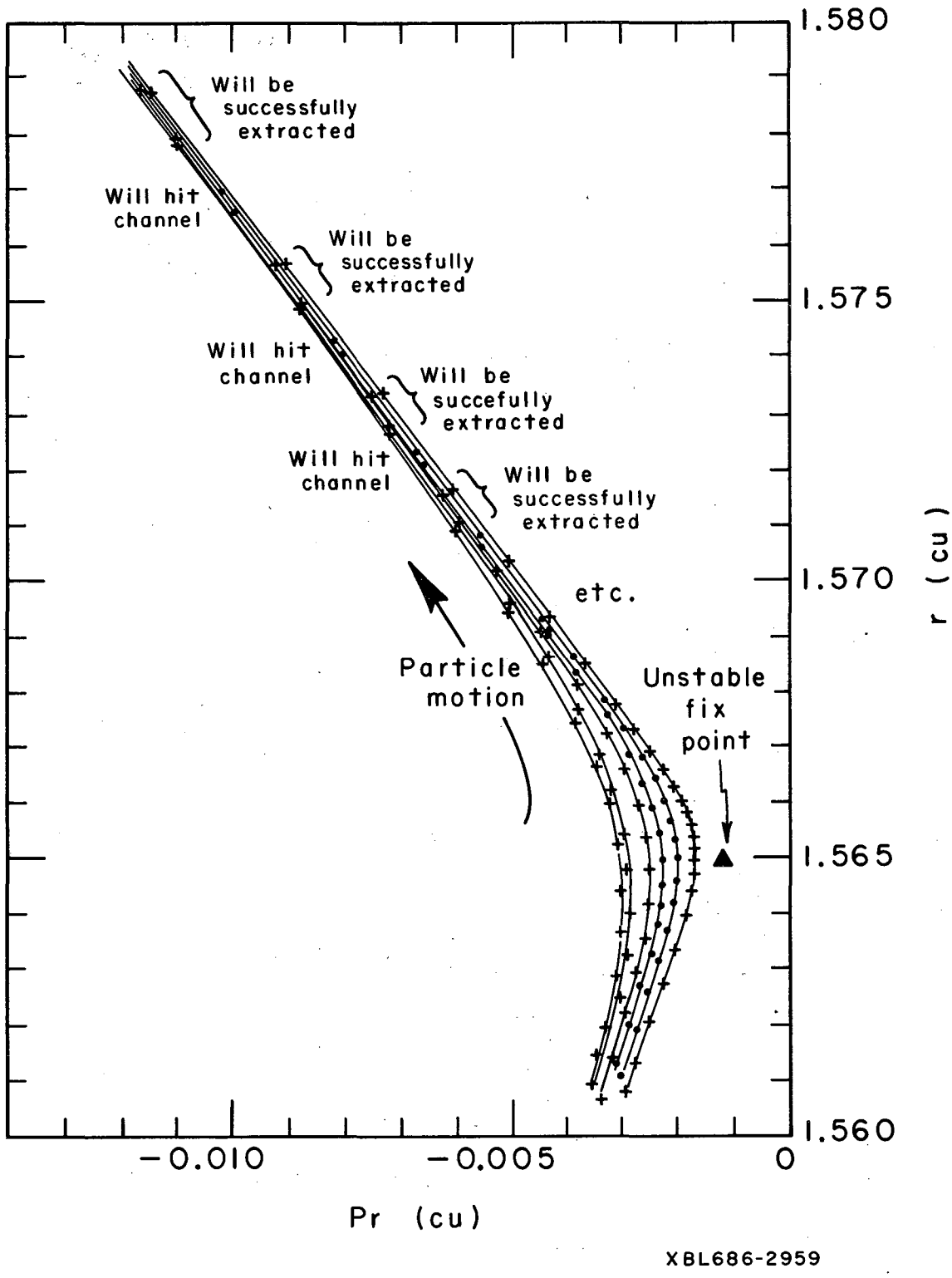

Fig. 9(b). Expanded portion of radial betatron phase space tail shown in Fig. 9(a).

connected the points with a line and indicate the regions between points where certain particles will suffer loss at other azimuths due to the indicated mode, Fig. 9(a).

The number of successful extraction bands is determined by the rate at which the particles gain energy and, therefore, how close they approach the unstable fix point. The total number of particles is independent of the rate of energy gain per turn. Experimentally, it is found that the extraction efficiency is about the same for the stretched beam as for the fast spill beam and therefore does not depend on the rate of energy gain per turn.

Figure 10(a) shows the 730-MeV radial phase space diagram on the same scale as the 700-MeV diagram. The future of an unsuccessful particle's beginning precessional motion after nearly completing regeneration is also indicated. This particle precesses rapidly about a second stable fix point corresponding to an equilibrium orbit on the back of the regenerator. Of course, this precessional particle is not executing oscillations about this equilibrium orbit. After comparatively few revolutions, these particles either blow up vertically or encounter the regenerator azimuth at a favorable phase so as to be knocked out of the magnetic field.

The phase space diagrams discussed so far and shown in Figs. 7, 8, 9(a), 9(b), and 10(a) are at a fixed azimuth with particle motion shown as the locus of points at that azimuth for each revolution. One can equally well follow the particle motion around the phase diagram in time (azimuth) as shown in Figs. 10(b) and (c). Here a 730-MeV particle of 1/4-in. initial vertical amplitude has been accelerated into regeneration. The radial and vertical betatron phase space motion is shown for the last three complete revolutions in the cyclotron before the particle escapes from the magnetic field. In regenerative build-up of the radial oscillation amplitude is apparent. The build-up of the vertical oscillation amplitude by deep penetration into the peeler is seen in Figs. 10(c) and 23(b).

V. CALCULATION OF THE EXTRACTION EFFICIENCY

Each particle, K_j, tracked in the computer is distinguished by the specification of the initial values of the four parameters of integration: energy $E(r)$, radial betatron phase $\theta(r,P_r)$, vertical betatron amplitude z, and vertical betatron phase $\Phi(P_z)$. A symbolic parameterization for the jth particle gives:

$$K_j \equiv K_j(E,\theta,z,P_z) \ .$$

Let a superscript o indicate the initial particle before acceleration and extraction. The vertical phase space for a particle of energy E and radial phase θ is then represented by the two vertically conjugate particles o_{K_j}, $o_{K_j}^*$ shown in Fig. 11 where * indicates the particle initially started with $z = 0$. If we choose

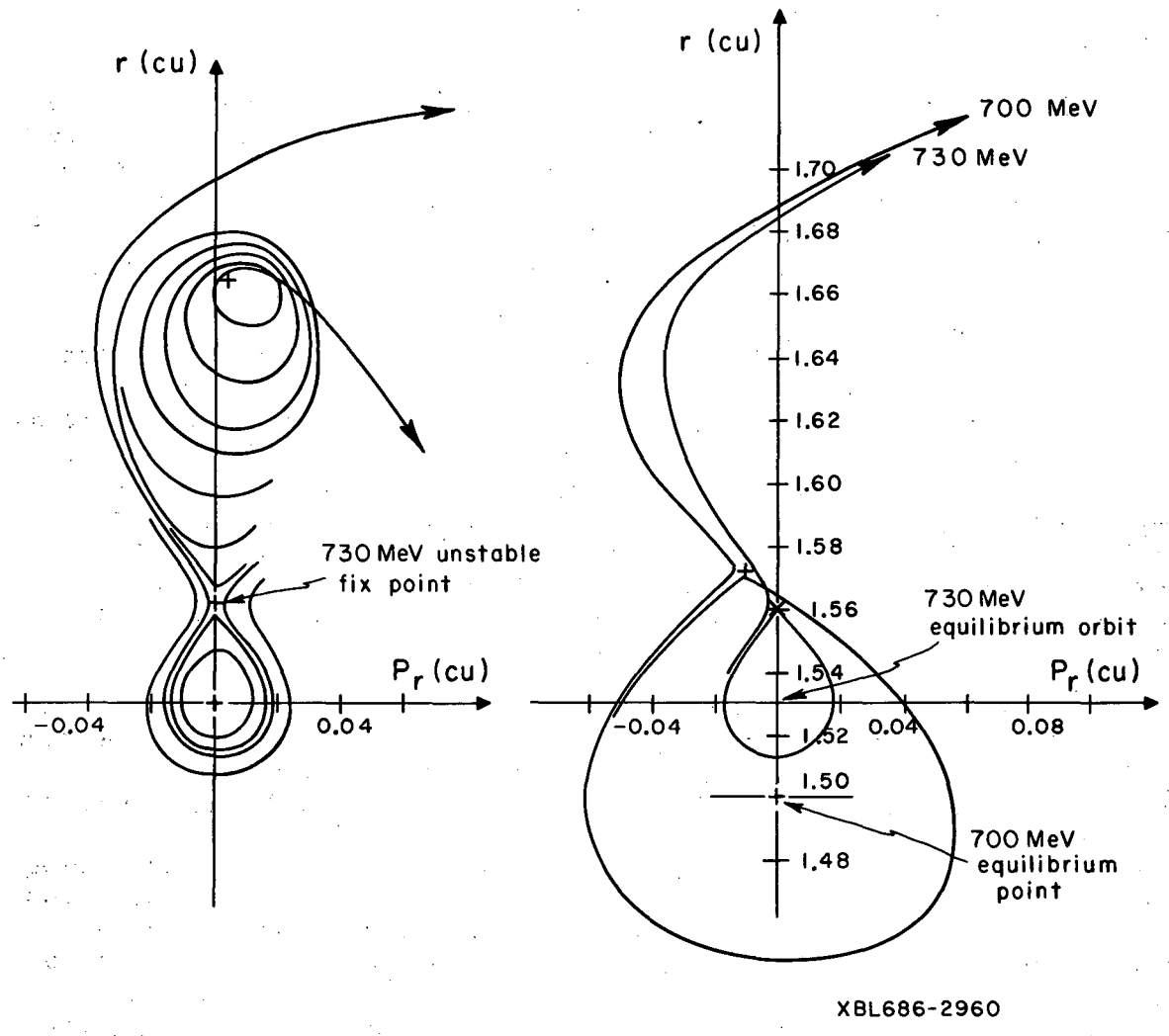

Fig. 10(a). 730-MeV radial betatron phase space showing comparison with 700-MeV phase plot.

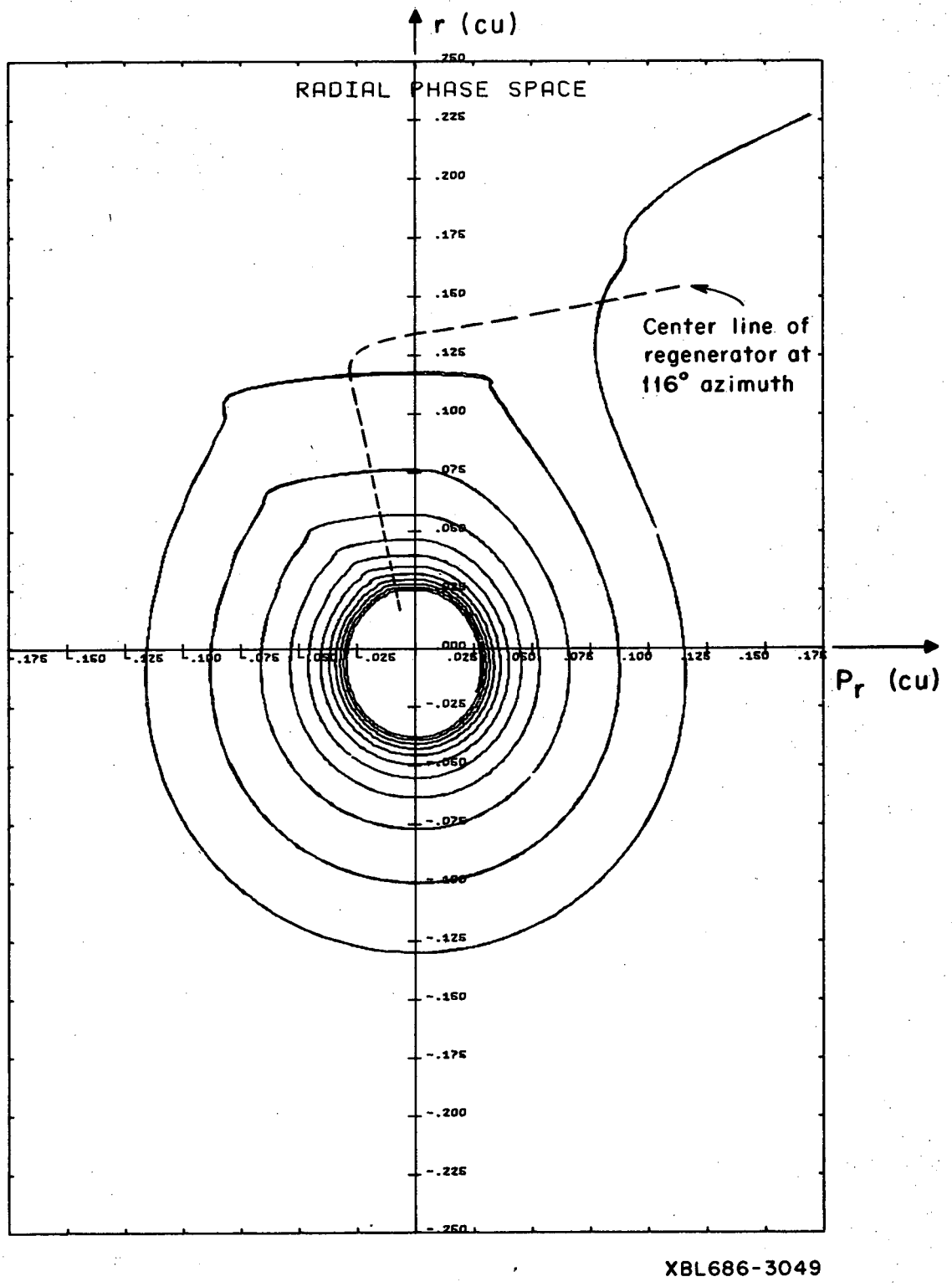

Fig. 10(b). Regenerative buildup of the radial betatron oscillations for a 730 MeV 1/4-in. vertical amplitude conjugate pair. The center line of the regenerator at 116° azimuth is shown. The concurrent vertical phase space motion is shown in Fig. 10(c).

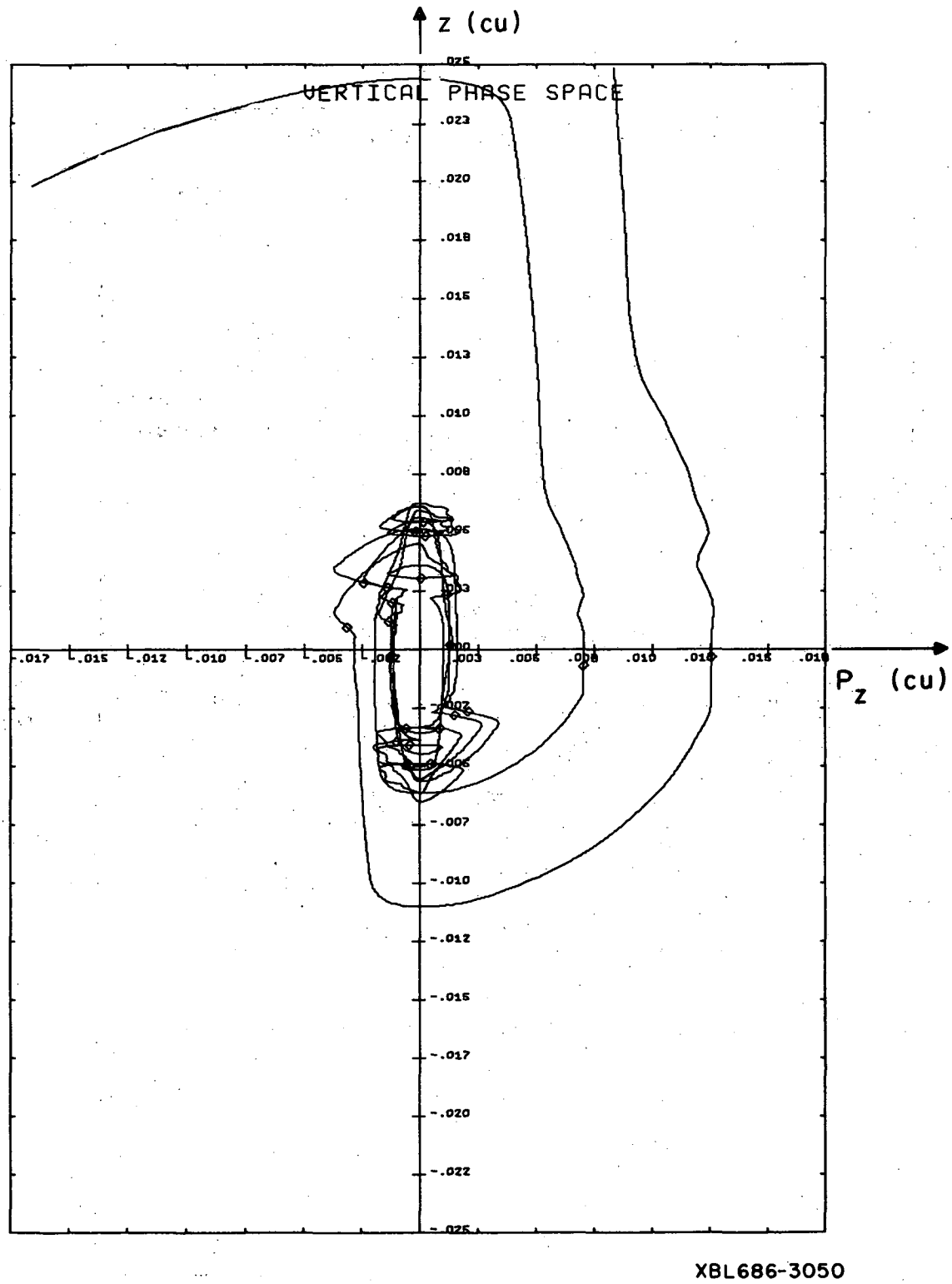

Fig. 10(c). "Peelerative" buildup of the vertical betatron oscillations for the 730 MeV conjugate pair whose radial motion is shown in Fig. 10(b). The initial vertical amplitude was 1/4 inch. The diamond (◇) markers indicate the center of the regenerator. The vertical amplitude vs azimuth for this conjugate pair is shown in Fig. 23(b).

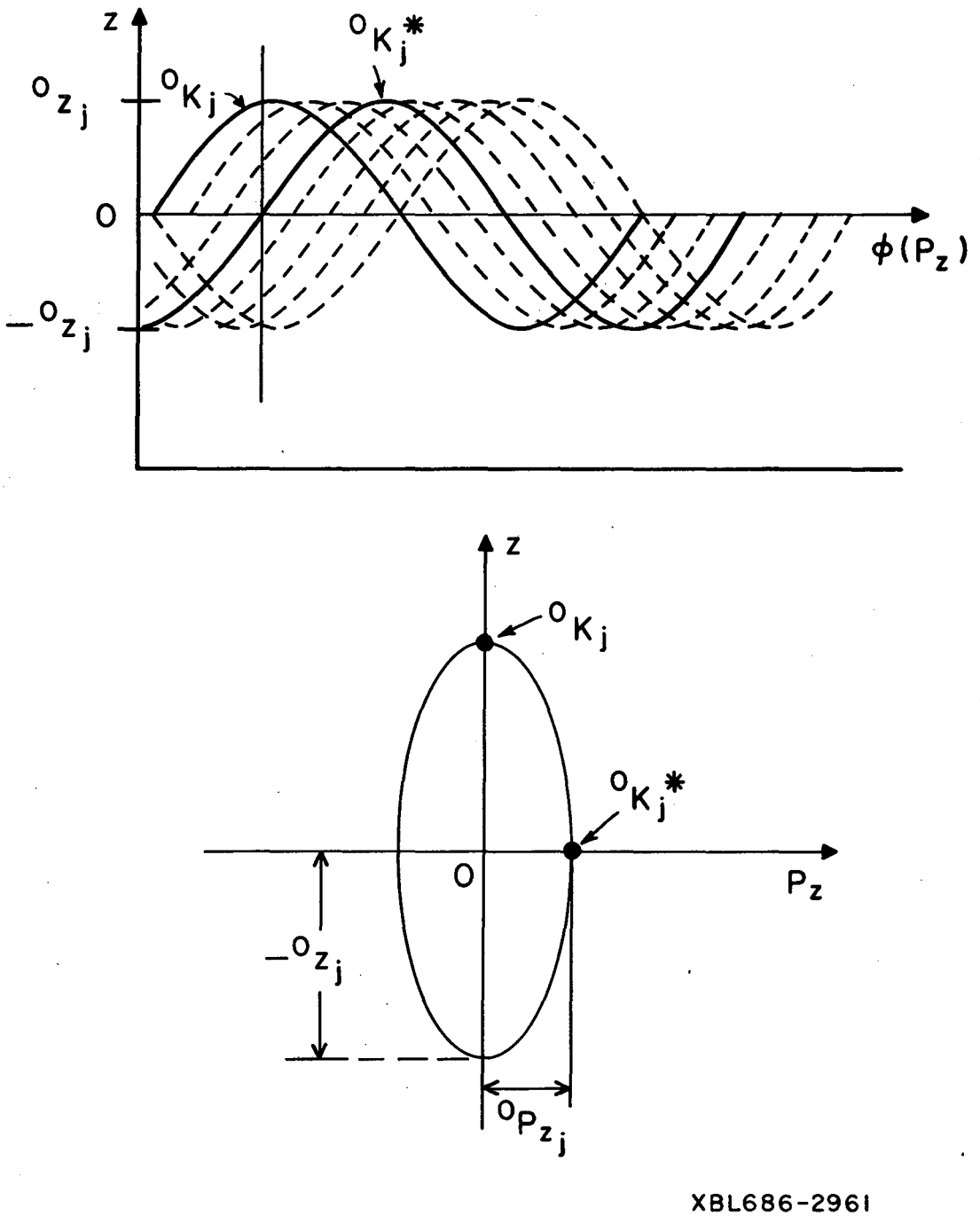

Fig. 11. Starting vertical phase space showing conjugate particle pair.

$$ {}^{o}P_{z_j}^{*} \equiv \left(\frac{{}^{o}z_j n^{1/2}}{r} \right) P \ , $$

where P is the momentum corresponding to E, we find that ${}^{o}P_{z_j}^{*}$ gives the same initial vertical oscillation amplitude as ${}^{o}z_j$. Then

$$ {}^{o}K_j \equiv {}^{o}K_j(E,z,0,\theta) \ , $$

$$ {}^{o}K_j^{*} \equiv {}^{o}K_j(E,0,P_z,\theta) \ . $$

These two particles, ${}^{o}K_j$ and ${}^{o}K_j^{*}$, comprise a vertically conjugate pair. The sum of these conjugate particle pairs over the radial phases is the total number of starting vertical phase spaces at each energy and vertical amplitude:

$$ {}^{o}K_j \, {}^{o}K_j^{*} \equiv 1 $$

$$ n_o(E,z) \equiv \sum_j {}^{o}K_j \, {}^{o}K_j^{*} \ . $$

The number of conjugate pairs that begin regeneration is

$$ n_1(E,z) = n_o(E,z)[1 - \mu_1(E,z)] \ , $$

where $\mu_1(E,z)$ represents the fractional loss of beam by vertical blowup before regeneration (Mode 1). Particles which begin regeneration but fail to complete regeneration due to the onset of radial precession are lost by subsequent vertical blowup or escape from the magnetic field at the wrong azimuth. The fractional loss of these Mode 2 particles is reflected by the factor $\mu_2(E,z)$. The number of conjugate particles starting the last regeneration turn (turn N) is given by

$$ n_N(E,z) = n_o(E,z)[1 - \mu_1(E,z)][1 - \mu_2(E,z)] \ . $$

These particles represent a large fraction of the internal beam. We can define the regeneration efficiency to be

$$ R(E,z) \equiv \frac{n_N(E,z)}{n_o(E,z)} \ ; $$

i.e., the ratio of the number of particles starting the last revolution in the cyclotron to the number present before entry into the regenerator perturbation. Clearly

$$ R(E,z) = [1 - \mu_1(E,z)][1 - \mu_2(E,z)] \ . $$

This represents the fraction of particles not undergoing Mode 1 or Mode 2 loss.

Define the internal cyclotron phase space loss factors $\mu_4(E,z)$ and $\mu_3(E,z)$ giving the fractional passage through the effective vertical internal aperture of the cyclotron and the fractional passage through the radial magnetic focusing channel aperture. Their values reflect the relative importance of the Mode 4 loss due to the strong overfocusing of the peeler field and the relative importance of Mode 3 loss originating from the finite radial width of the channel. The beam passing through the magnetic channel is then

$$n_{N+1}(E,z) = n_o(E,z)\lambda(E,z) \ ,$$

where lambda is the differential emittance of the regenerator-cyclotron geometry representing the fractional emission of particles of energy E and amplitude z from the magnetic channel:

$$\lambda(E,z) = [1 - \mu_1(E,z)][1 - \mu_2(E,z)][1 - \mu_3(E,z)][1 - \mu_4(E,z)] \ .$$

The differential extraction efficiency $\eta(E,z)$ gives the energy and vertical amplitude dependence of the cyclotron-external beam geometry and represents the common phase space overlap between the differential cyclotron emittance and the radial and vertical external beam phase space acceptance factors $\delta_x(E,z)$ and $\delta_y(E,z)$:

$$\eta(E,z) = \lambda(E,z)\ \delta_x(E,z)\ \delta_y(E,z) \ ;$$

$\eta(E,z)$ is the percentage of particles at energy E with vertical amplitude z which satisfy the radial and vertical acceptance criteria for transmittal down the external beam line to the physics cave snout, Fig. 21. The actual number of particles at this energy and vertical amplitude is calculated by weighting the differential extraction efficiency by the number of particles in phase space, $\sigma(E,z) \equiv \sigma(E)\ \sigma(z)$:

$$n(E,z) = \eta(E,z)\sigma(E,z) \ .$$

The total number of particles successfully extracted in each energy interval is given by

$$n(E) = \int \eta(E,z)\sigma(E,z)\ dz \ .$$

This determines the energy distribution of the external beam. The total number of accelerated particles contributing to the external beam, n, is given by

$$n = \int n(E)\ dE \ .$$

The extraction efficiency ϵ is the ratio of n to the total number of starting particles N

$$\epsilon = \frac{\int n(E)\ dE}{\int \sigma(E,z)\ dE\ dz} \ .$$

VI. THE VERTICAL DISTRIBUTION

The number of particles per unit area in the vertical phase space is observed to be constant except for a tail at large amplitudes. The phase space area dA associated with an amplitude range z_1 to z_2 is the difference in area ($\pi z P_z$) between two ellipses of the same eccentricity, ϵ,

$$dA = \pi(1 - \epsilon^2)^{1/2}(z_2^2 - z_1^2) ;$$

if $z_2 = z_1 + dz$, then

$$dA = [2\pi(1 - \epsilon^2)^{1/2}\, dz]z .$$

The number of particles with amplitude z is proportional to the amplitude for a constant interval size dz.

The relationship between the phase space density $\rho(z) = dn/dA$ (number of particles per unit area) and the number of particles per unit amplitude $\sigma(z) = dn/dz$ is

$$\sigma(z) = \rho(z)\, 2\pi(1 - \epsilon^2)^{1/2} z .$$

The vertical amplitude distribution was measured with a rotatable finger probe limiting the beam height at 70 in. radius. The beam reaching 78 in. radius was measured by counting the neutrons produced by a target at that radius with a fission chamber as a function of the vertical amplitude (determined by distance between finger and median plane). Figure 12 shows the vertical phase space density remains approximately constant out to 5/8 in., dropping to zero at 7/8 in. with half maximum at 0.725 in. The distribution from the above equation for $z_{max} = 23/32$ is also indicated. Half of the internal beam at 70 in. radius as a vertical amplitude greater than 1/2 in.

VII. THE RADIAL DISTRIBUTION

The relation between the radial betatron amplitude determining the number of particles in the radial phase space and the energy of extraction is somewhat non-linear because the radius of the equilibrium orbit expansion varies with energy and the radial position of the point of start of regeneration is energy dependent. These effects are shown in Fig. 13. The number of particles $\sigma(E)$ within the energy interval E_i to E_{i+1} can be calculated from the radial interval r_i to r_{i+1} associated with this energy, Fig. 14:

$$\sigma(r) \propto (r_{i+1}^2 - r_i^2) ,$$

$$\sigma(E) = f(r,E)\, \sigma(r) ,$$

where $f(r,E)$ is a numerically determined relation between the energy where a given radial betatron oscillation amplitude reaches 81.5 in. and the energy of the start of regeneration.

The radial betatron phase space distribution was measured by

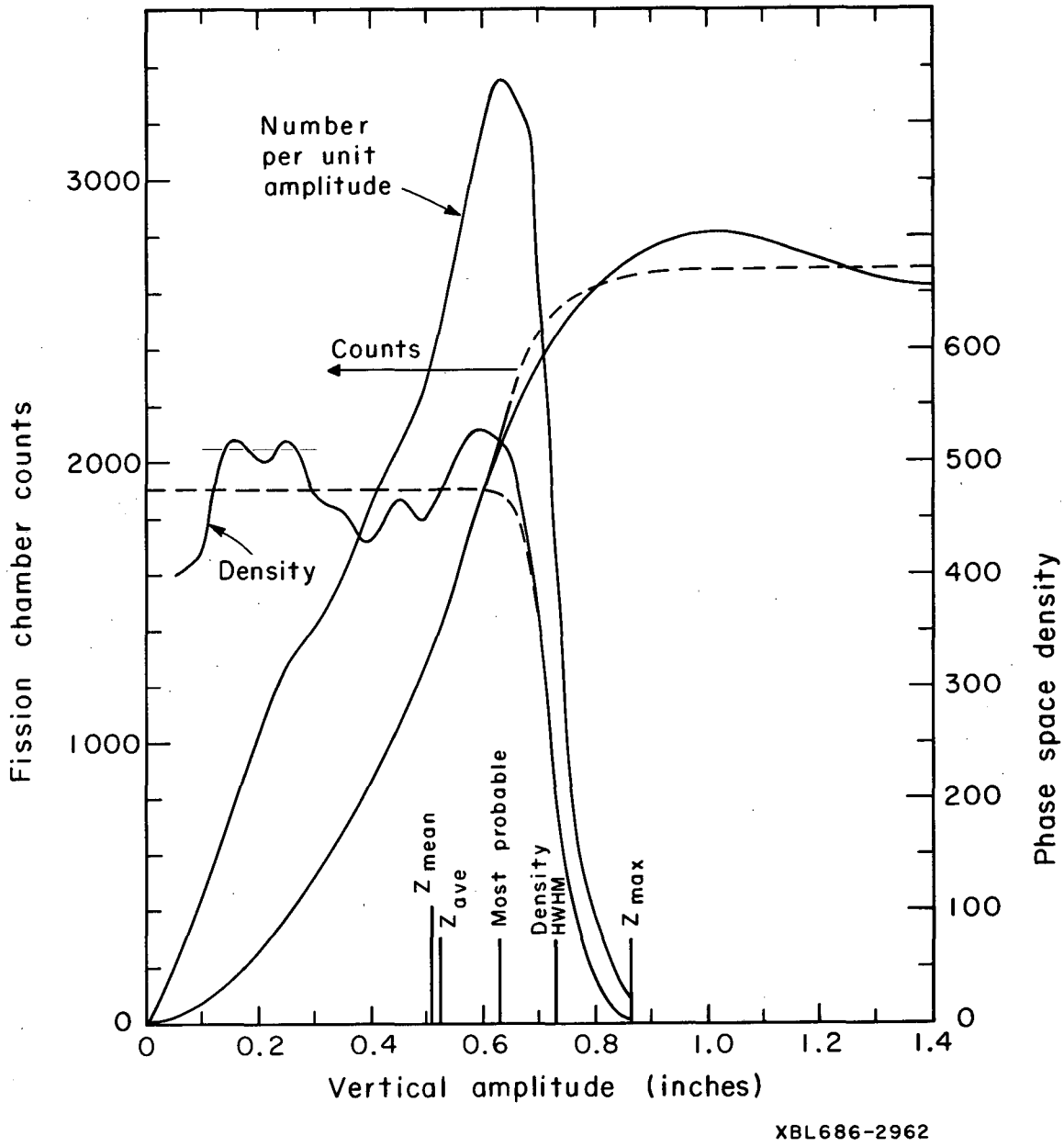

Fig. 12. Measured vertical phase space.

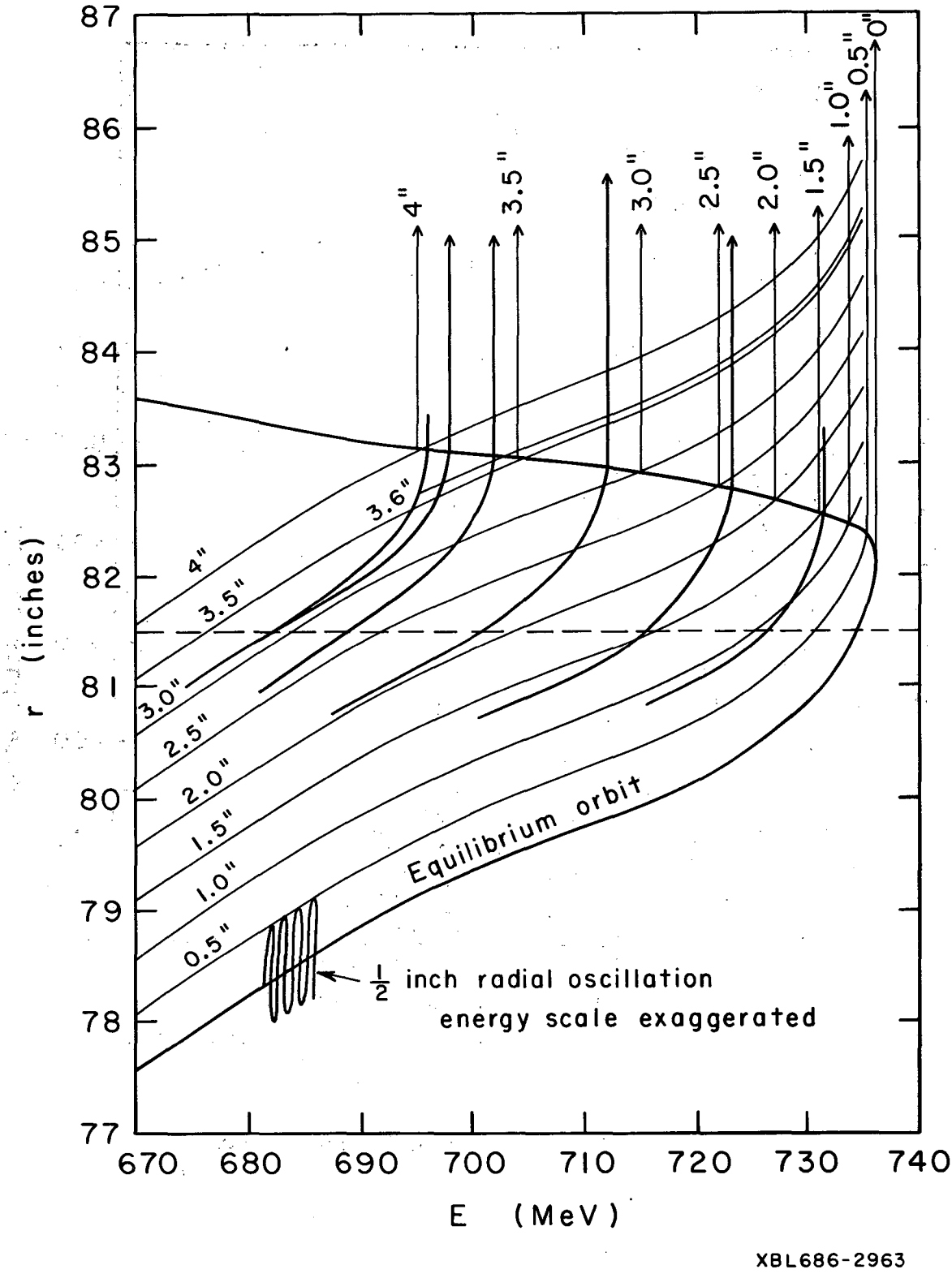

Fig. 13. Radial motion of particles at 116° azimuth, showing effect of regenerator.

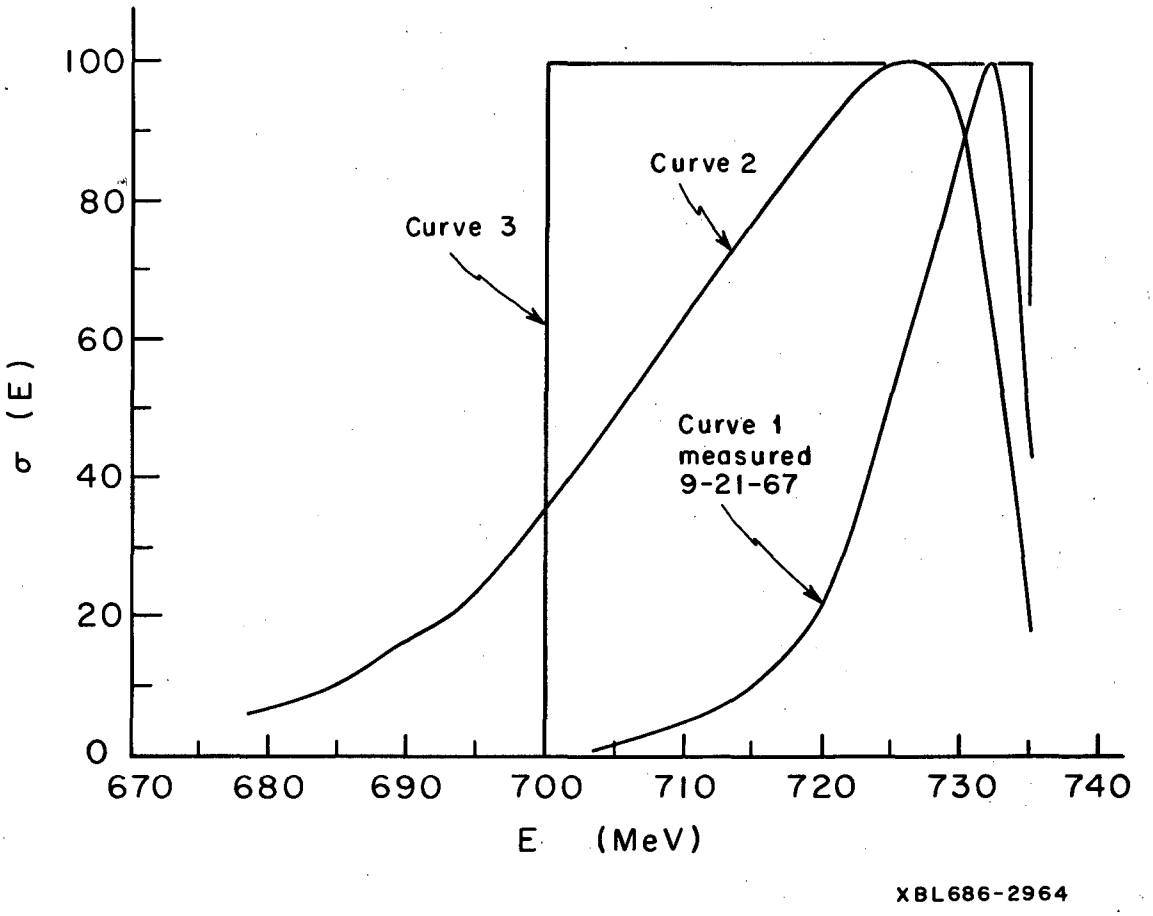

Fig. 14. Number of particles per unit energy. Measured curve of 9-21-67 and curves 2 and 3 used in calculating Fig. 25.

observing the time dependence of the output of a scintillator looking at a target at 78 in. radius. This time dependence was converted to a radial dependence from the known relations between measured frequency and time and radius versus frequency (inferred from the magnetic field as a function of radius). The results are shown in Fig. 15. The distribution seems to be approximately gaussian to within experimental error, Fig. 24, and characterized by an increasing density out to about 1/4 in., then constant density to 1 in., dropping to zero at 3 in. with a half-maximum value at 1-1/2 in. Normal operation at present yields this 3 in. maximum radial oscillation amplitude. Oscillation amplitudes of up to 6 in. have apparently been observed under certain operating conditions with a reported extraction efficiency of 5%.[22]

VIII. EXTERNAL BEAM ACCEPTANCE FACTORS

The orbit calculations end inside the cyclotron fringing field at 106 in. radius, 166-172 deg azimuth. The field here is approximately 5000 G. The subsequent particle trajectories are not calculated through the remaining fringing field. Rather, the matrix from the cyclotron orbit exit (106 in., 166 deg), along the optic axis through the fringing field to each element of the external beam line, is calculated for typical values of operating field of the various external beam magnets.[23] These matrices are then inverted so that the vertical and horizontal apertures of the external beam magnets can be transformed backward to the phase space at the end of the cyclotron calculations (106 in., 166 deg). These transformed apertures drawn in the emittance phase space of the cyclotron, determine the regenerated particle contribution to the external beam for each starting energy and amplitude, Figs. 16 and 17, and determine the radial and vertical acceptance factors, $\delta_r(E,z)$ and $\delta_z(E,z)$. The apparent 90-deg rotation between the radial acceptance and emittance may reflect the non-tuned operation described by the magnetic field used in the calculations. This field is approximately 100 G low (see Section I). The actual field of the machine is tuned for maximum transmission, which at the higher excitation and saturation may rotate the figures into better alignment.

IX. ORBIT CALCULATIONS

Particle orbits were calculated with a General Orbit Code[24] in the magnetic field of the 184-in. cyclotron. Approximately 1500 particles

---

[22] Ken Crowe, "Conference on High Energy Cyclotron Improvement," College of William and Mary, 108 (1964).

[23] L. Moore, S. Howry, H. Butler. TRANSPORT, A Computer Code for Designing Beam Transport Systems, Stanford Linear Accelerator Report (1964).

[24] D. I. Hopp, "General Orbit Code," UCLA Technical Report P-67 (1965), based on Gordon and Welton, ORNL-2765 (1959).

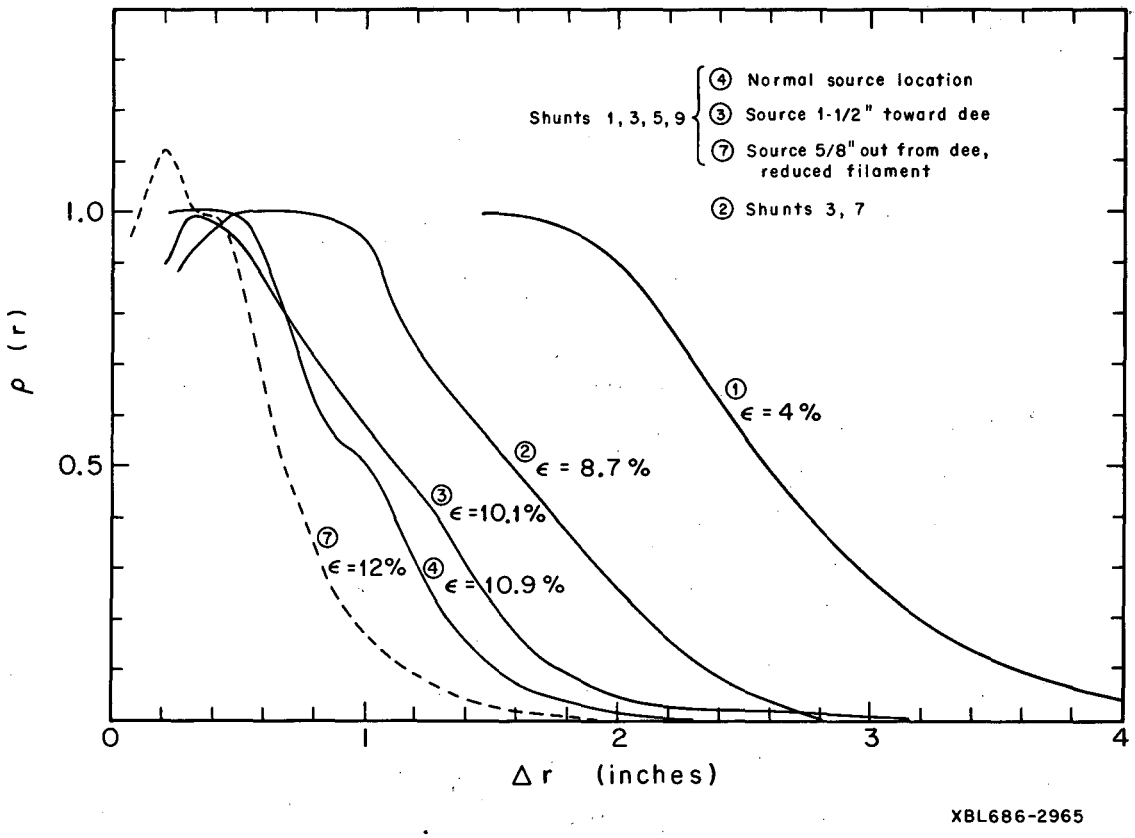

Fig. 15. Measured radial phase space density.

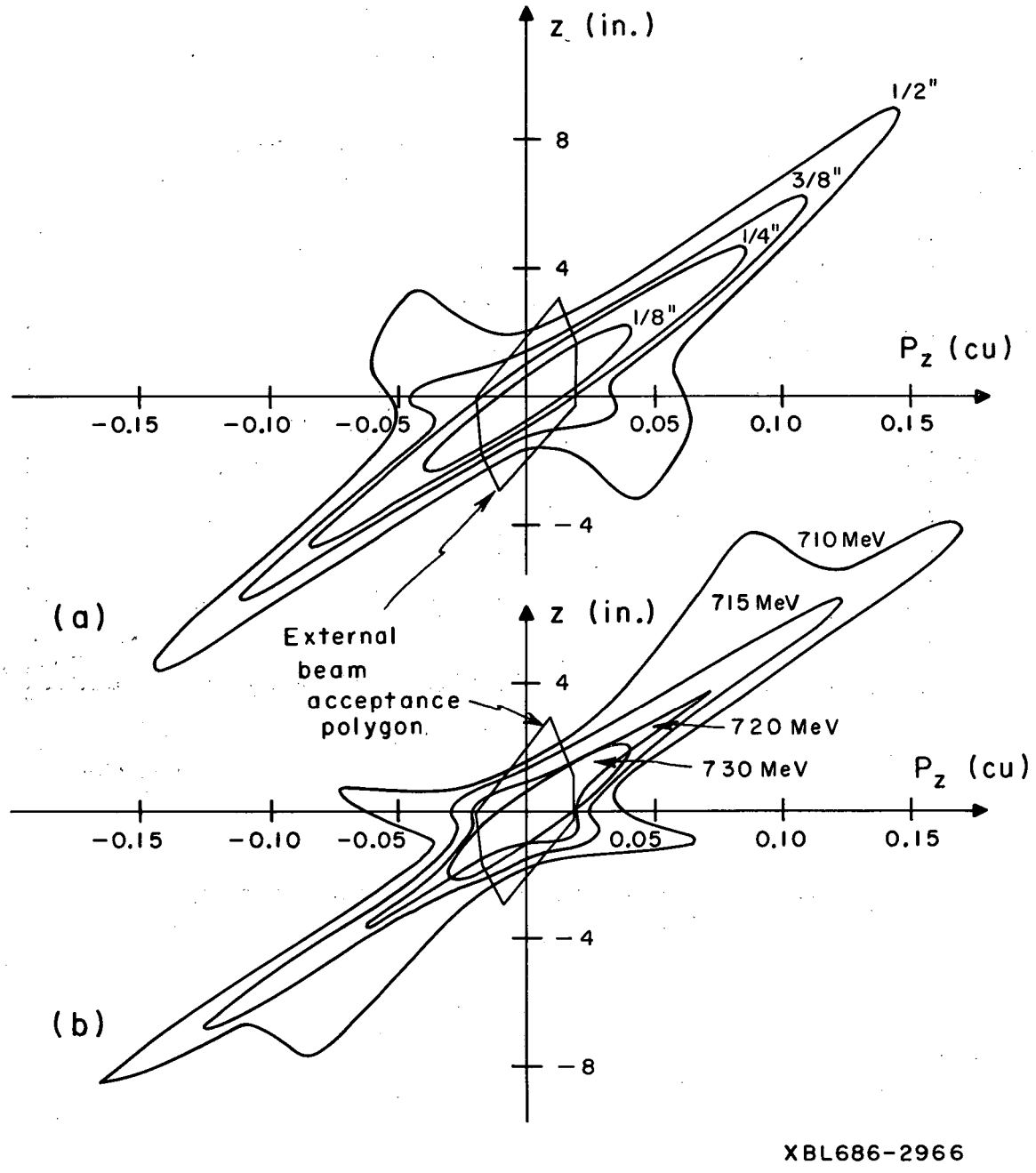

Fig. 16(a). Calculated 730-MeV vertical phase space at 106" 166° for z_{amp} = 1/8, 1/4, 3/8, and 1/2 in.
(b). Calculated 1/8-in. vertical phase space at 106" 166° for E = 730, 720, 715, and 710 MeV. No vertical or radial internal apertures.

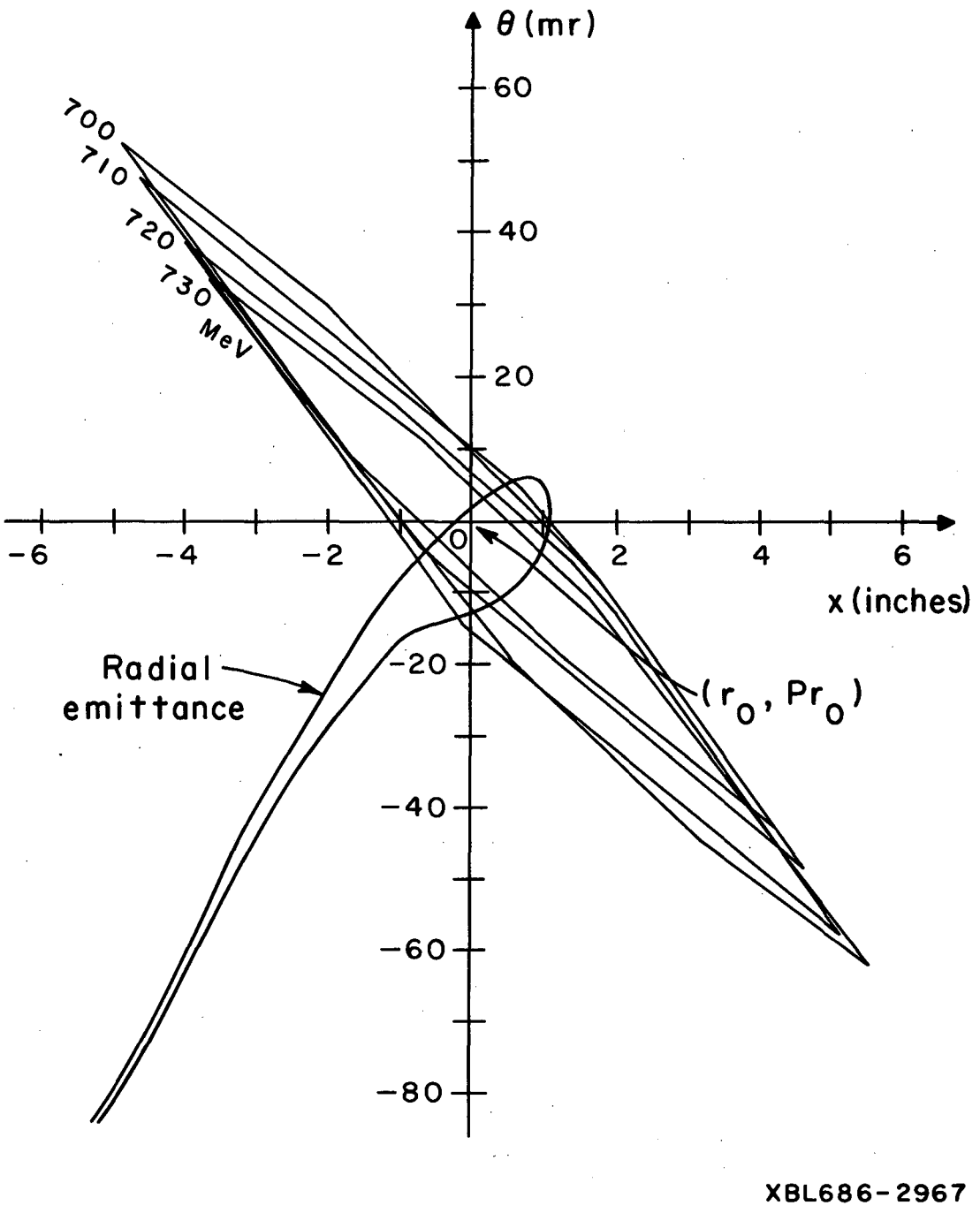

Fig. 17. Radial phase space at 106" 160° showing external beam acceptance polygons.

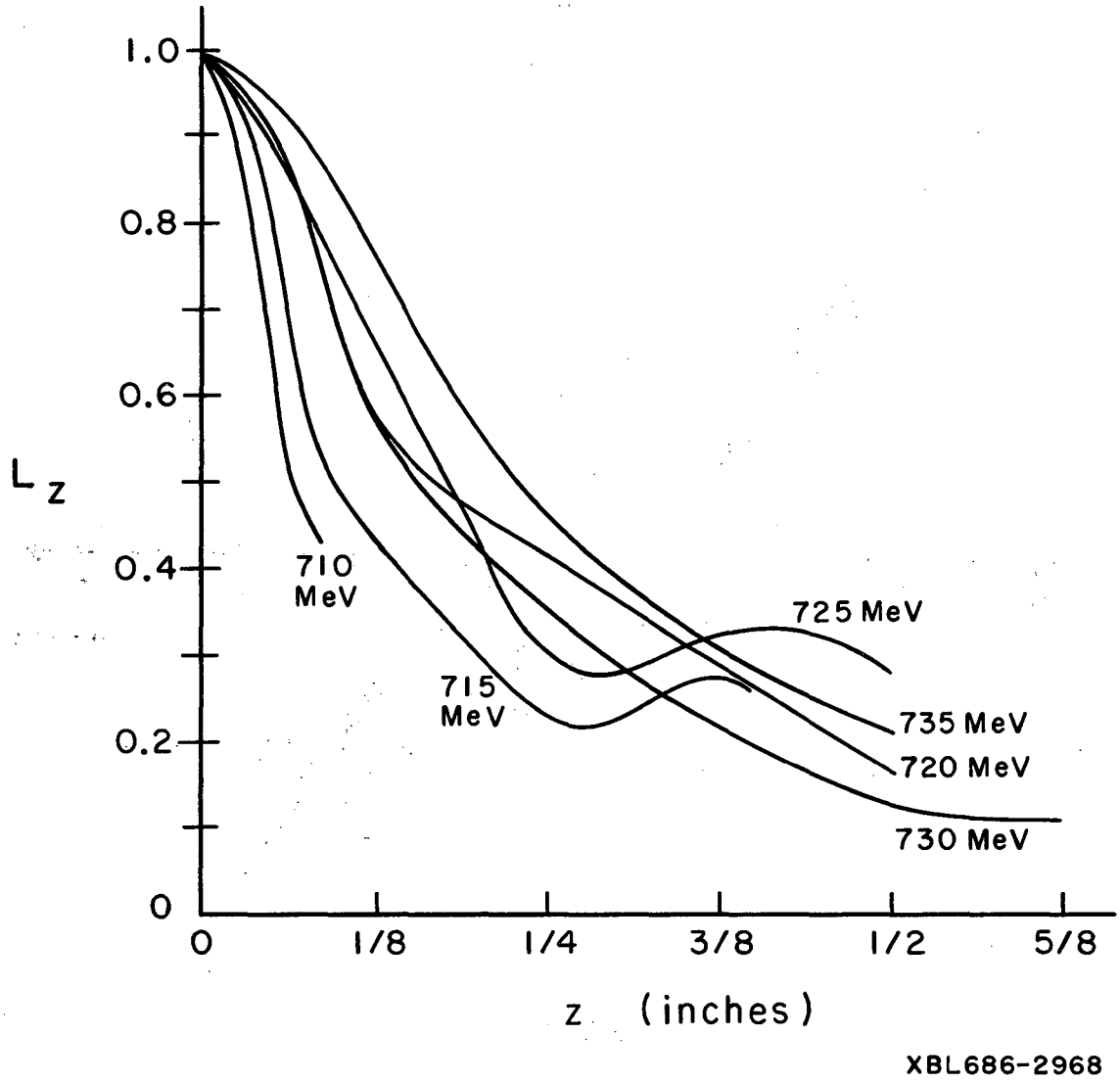

Fig. 18. Vertical loss factor $L_z = (1 - \mu_4)\,\delta y$.

were started inside the stable region of the radial betatron phase space and accelerated through at least one complete precessional oscillation (40-100 revolutions) before gaining sufficient energy to cross the separatrix of the phase space diagram, Fig. 9(a). During this precessional revolution they sample entry into the regenerator without extraction. Once outside the stable region, regeneration sets in with the cessation of the radial betatron precession and the radial amplitude begins to grow. The calculations stop when the particles are about 2 in. from the end of the magnetic field in the computer memory (108-in. radius) or have a vertical amplitude larger than 100 in. Particles which have successfully negotiated the magnetic channel are between 166-172 deg azimuth at 106 in. radius.

The resulting fate of the particles started in the computer is shown in Tables 4 and 5. Here particles listed under no loss, some loss, and severe loss meet the magnetic channel radial acceptance criteria with the indicated degrees of vertical acceptance. Particles which begin regeneration but do not complete it are listed under precession and are characterized by orbits of type B of Fig. 6 (Mode 2 loss). Particles which are extracted but fail the channel acceptance criteria are listed under "hit channel" (Mode 3 loss). Particles which never begin regeneration are lost vertically at low energy (Mode 1 loss which occurs at less than 715 MeV and corresponds to a large radial oscillation amplitude). These various modes of loss occur at distinct regions of the phase space diagram, as shown in Fig. 9(a).

The calculated regeneration efficiency, $R(E,z)$, is shown in Fig. 19. Seventy-five percent of the internal beam is successfully regenerated to the last two turns as found by integrating $R(E,z)$ over the observed particle distribution $\sigma(E,z)$ (Mode 1 and 2 loss only):

$$\epsilon_R = \frac{\int R(E,z)\sigma(E,z)\, dE\, dz}{\int \sigma(E,z)\, dE\, dz} = 75\% .$$

The calculated differential extraction efficiency $\eta(E,z)$, including Mode 1, 2, 3, and 4 losses, is shown in Figs. 20 and 21. We can hypothetically remove the vertical restrictions by setting $\delta_y = 1$, $\mu_4 = 0$. This would correspond to correction of the vertical overfocusing in the peeler (Mode 4). The extraction efficiency ϵ then amounts to 32%. Figure 22 shows

$$[1 - \mu_1(E,z)][1 - \mu_2(E,z)][1 - \mu_3(E,z)]\delta_x(E,z)$$

as a function of energy and vertical amplitude. This figure should be compared to Fig. 21 where $\delta_y \neq 1$ and $\mu_4 \neq 0$.

Figure 23(a) shows a vertical phase space ellipse at 116 deg azimuth typical for all initial vertical amplitudes satisfying the radial external beam acceptance criteria. This group of particles sampled one complete radial precession before regeneration and regenerated through turn 90 without significant increase in the axial displacement. No loss of particles has occurred. Turn 92 is the last revolution where the

Table 4. Complete channel acceptance.

Energy (MeV)	Amplitude vertical (in.)	No vertical loss	Some vertical loss	Severe vertical loss	Mode 1 loss	Mode 2 loss	Partial mode 3 loss	Total number of particles
735	0	20	0	0	0	7	16	43
	1/4	10	6	0	0	6	21	43
	1/2	2	4	7	0	8	22	43
730	0	25	0	0	0	0	18	43
	1/8	17	6	0	0	2	18	43
	1/4	4	18	0	0	6	15	43
	3/8	0	18	3	0	6	16	43
	1/2	1	4	14	0	10	14	43
	3/4	0	5	13	0	14	11	43
725	0	29	0	0	0	--	--	44
	1/8	18	0	0	--	12	14	44
	1/4	6	7	0	--	17	14	44
	1/2	--	--	--	--	--	--	0
720	0	29	0	0	0	6	14	49
	1/8	7	2	0	--	9	7	25
	1/4	6	8	0	--	3	8	25
	1/2	0	5	7	--	4	9	25
715	0	16	0	0	0	1	14	31
	1/16	8	9	0	--	1	13	31
	1/8	4	7	0	--	2	18	31
	1/4	3	2	4	2	9	13	31
	3/8	2	3	4	--	4	17	31
	1/2	--	--	--	--	--	--	0
710	0	--	--	--	--	--	--	0
	1/16	6	2	4	--	6	11	29
	1/8	3	2	2	--	9	13	29
	1/4	--	--	--	0	7	12	31
700	0	12	0	0	0	7	12	31
	1/16	0	0	0	15	16	0	31

Table 5. Calculated differential regenerator transmission (%).

E(MeV)/z(in.)	735	730	725	720	715	710	705	700
3/4	--	5.						
11/16								
5/8								
9/16								
1/2	7.	5.	10.	7.				
7/16								
3/8	--	11.	--	--	8.			
5/16								
1/4	17.	17.	7.	24.	6.			
3/16								
1/8	--	30.	27.	20.	15.	10.		
1/16	--	--	--	--	28.	21.	--	0.
0	46.	58.	66.	59.	52.	--	--	39.

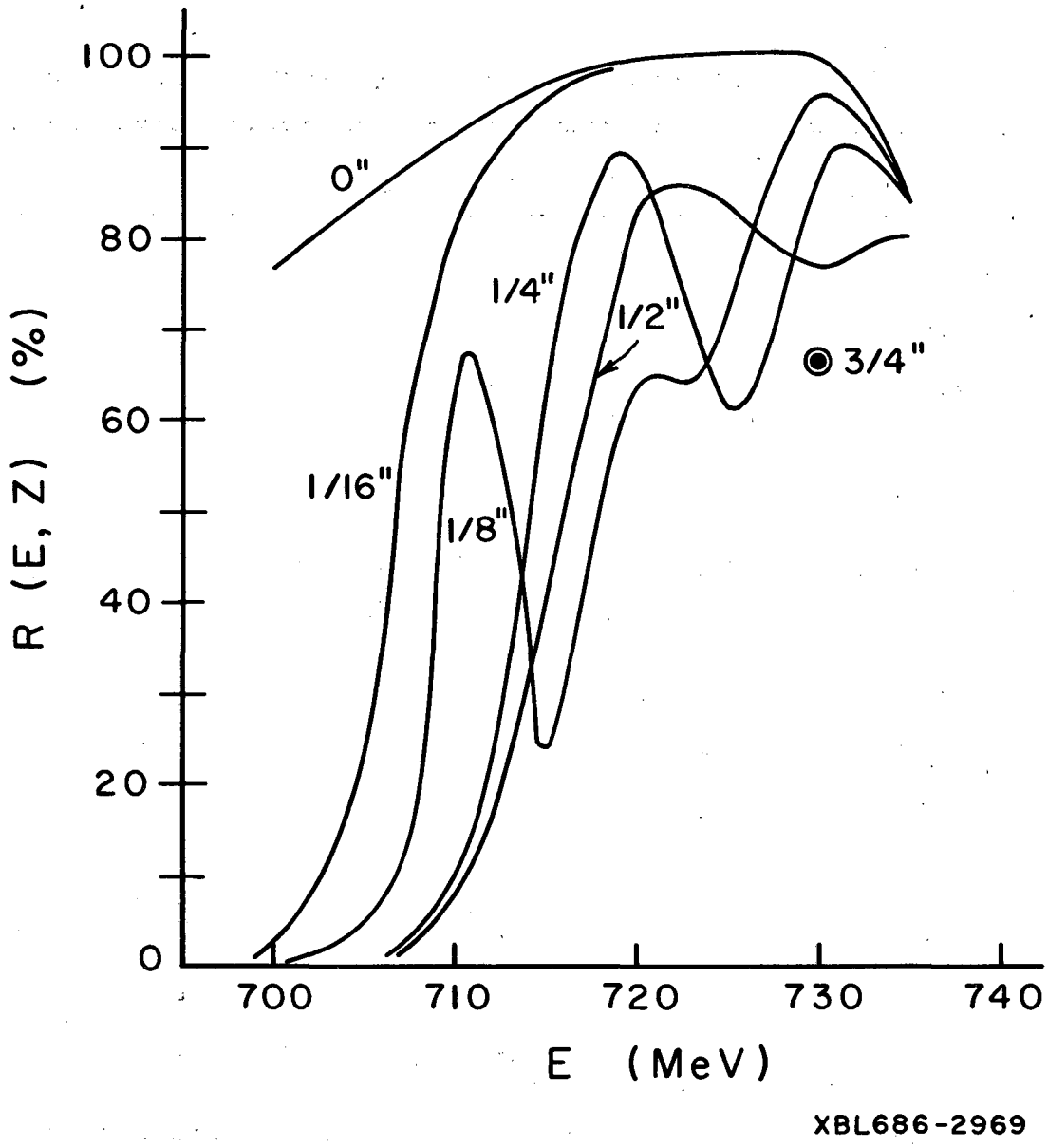

Fig. 19. Regeneration efficiency as a function of the vertical oscillation amplitude.

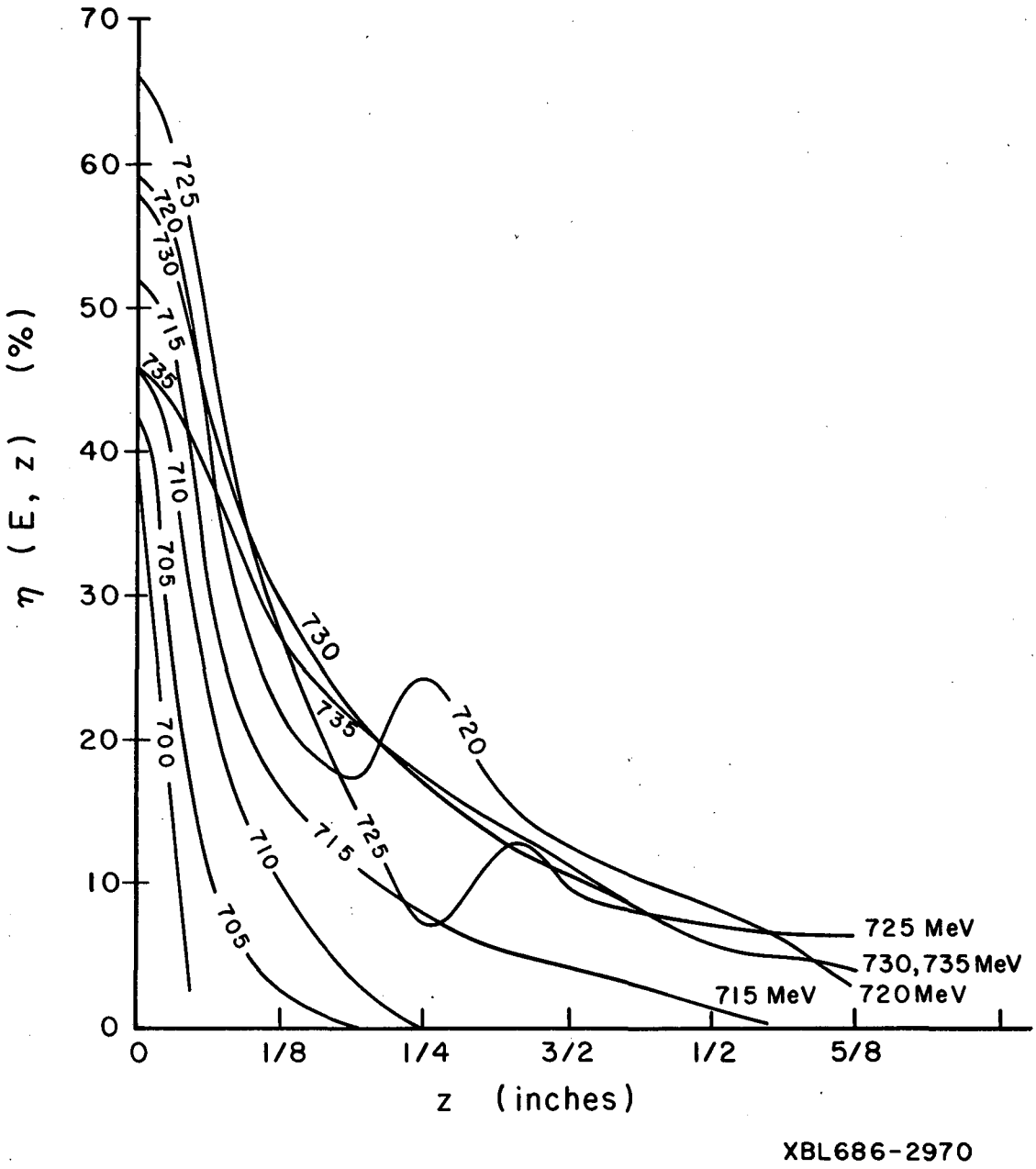

Fig. 20. Differential extraction efficiency $\eta(E, z)$ in the E plane.

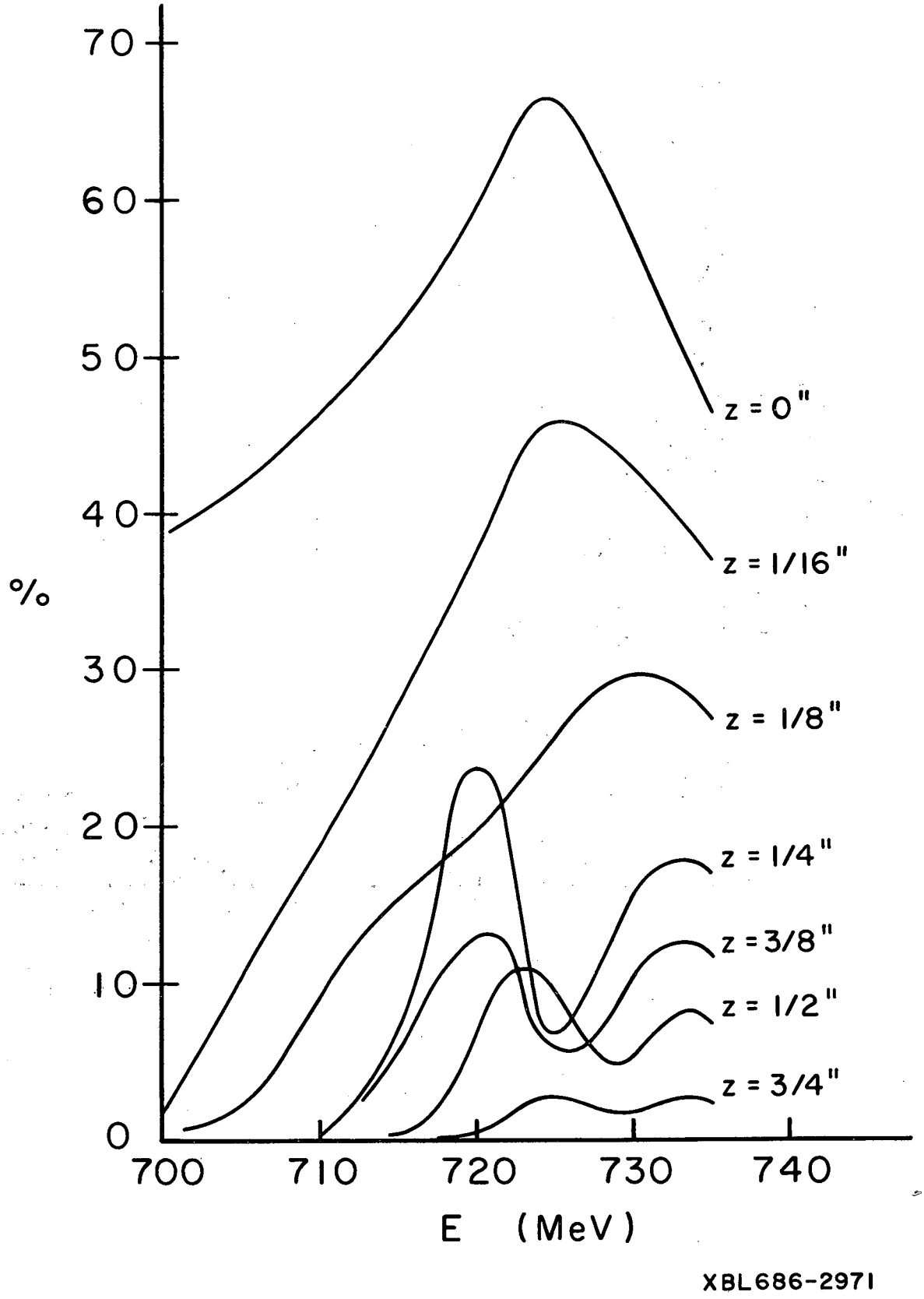

Fig. 21. Differential extraction efficiency $\eta(E, z)$ in the E plane.

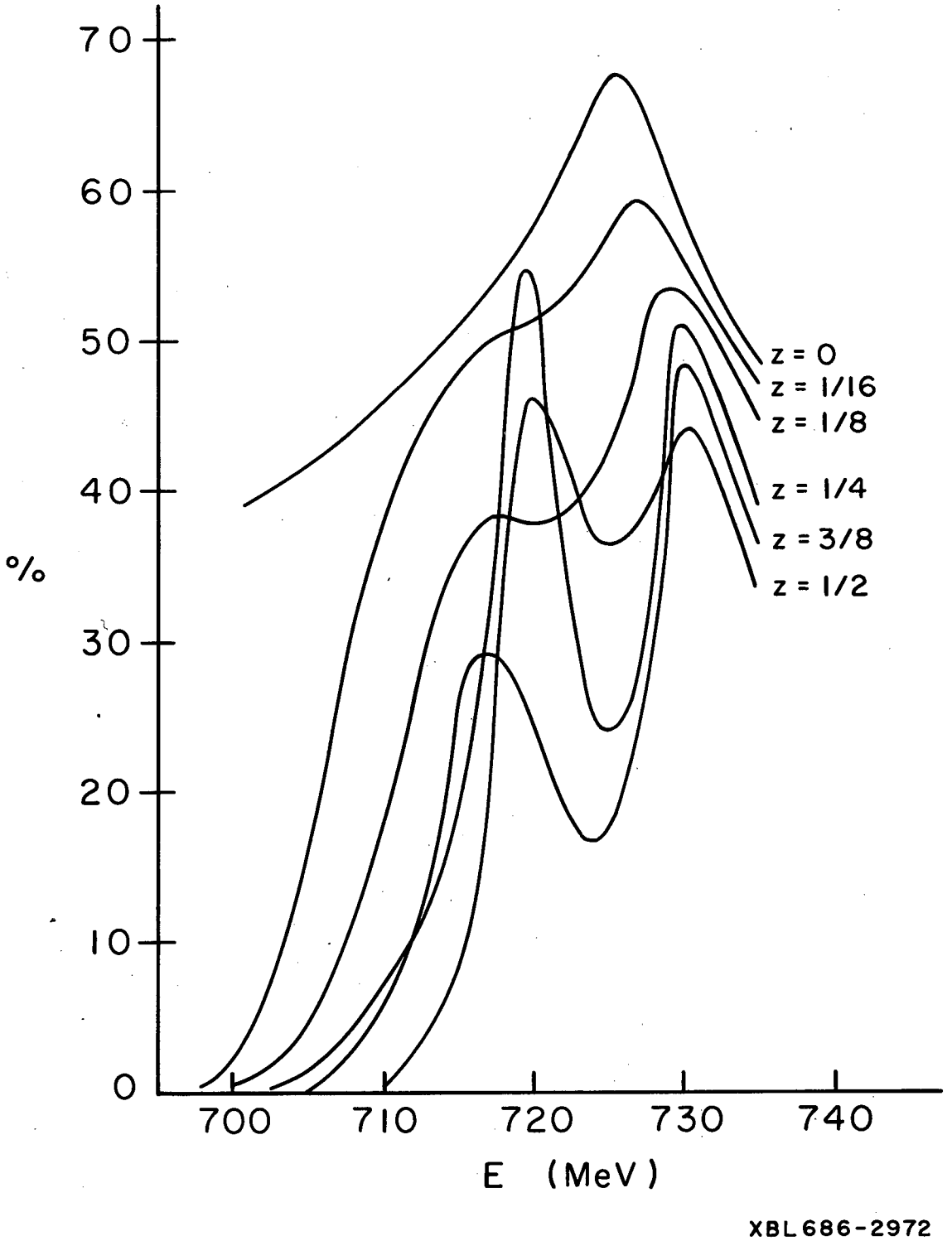

Fig. 22. Regenerated beam with no vertical restrictions.

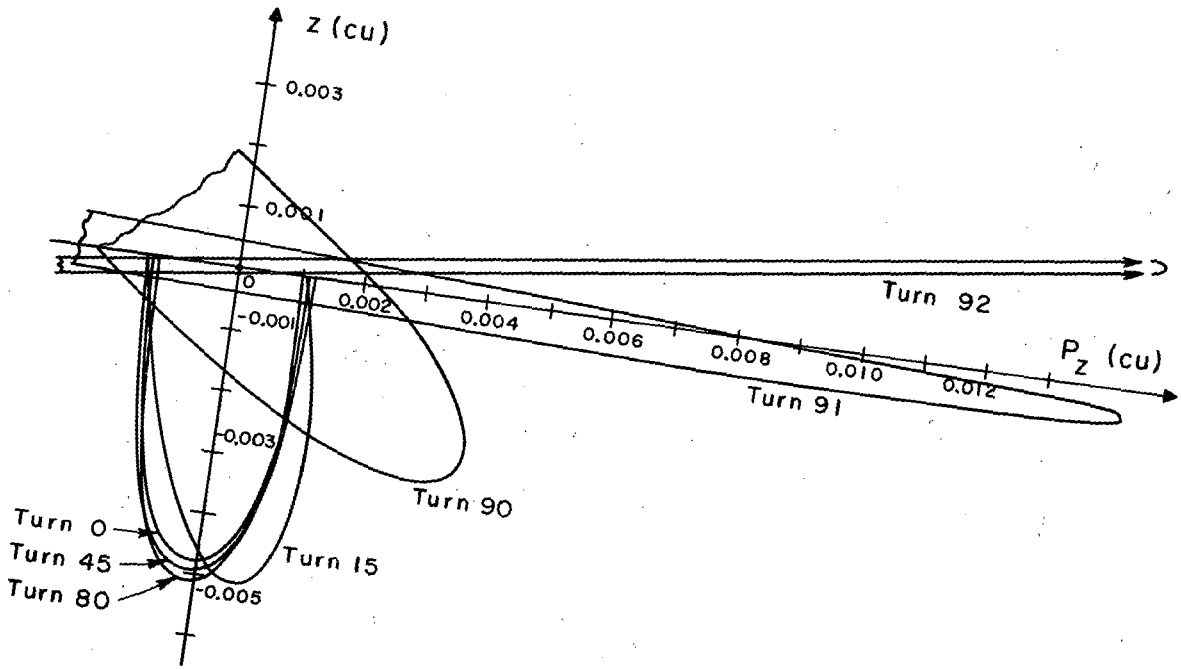

Fig. 23(a). 730-MeV, z = 1/4-in. vertical phase plot at 116° azimuth.

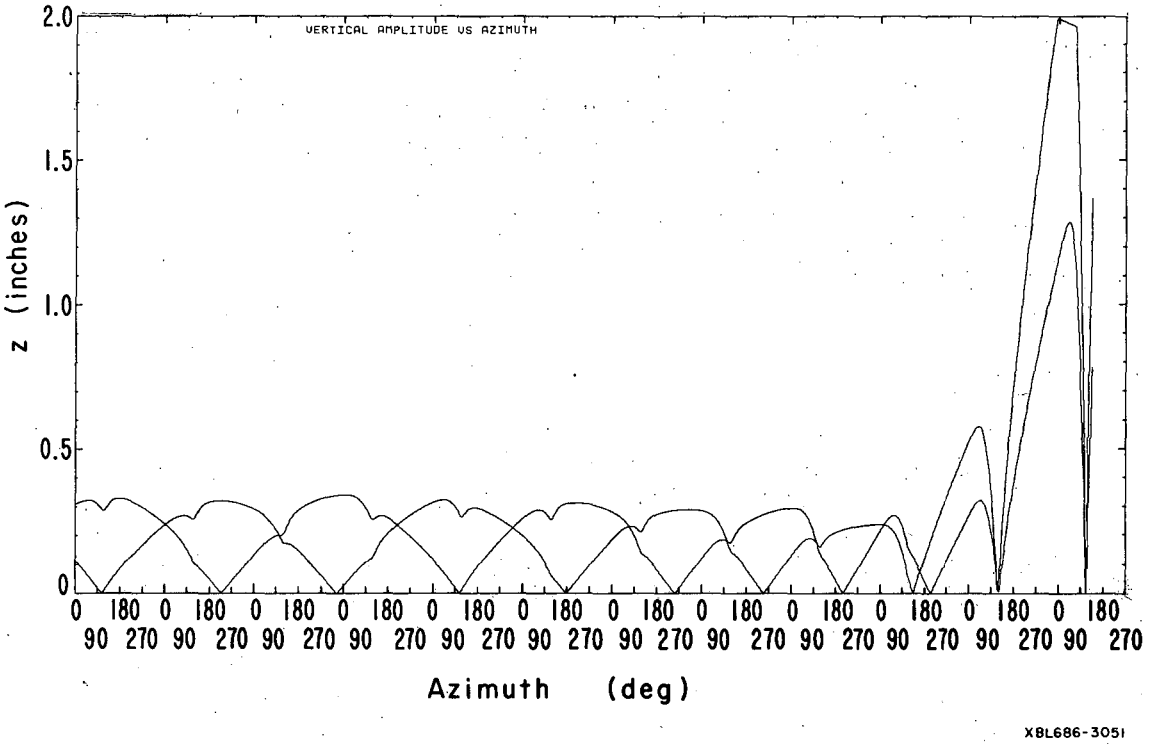

Fig. 23(b). The vertical amplitude vs azimuth for the conjugate particle pair whose phase space motion was shown in Figs. 10(b) and (c). The vertical defocusing of the regenerator is noticeable at 116°. Note also the $\nu_z = 1/2$ resonant buildup of the vertical amplitude.

particles have been brought to a strong vertical focus at 105 deg. Although the displacement of these particles is nowhere more than 3/8 in. before revolution 90, they will be displaced by 4 in. from the median plane at the face plate of the cyclotron and will suffer severe loss by the time they reach the quadrupole. The problem is clearly identified with vertical overfocusing during the last few revolutions in the peeler. This can be seen in the real space representation of Fig. 23(b) showing the vertical amplitude versus azimuth for two particles of the same initial energy and vertical amplitude, but differing in vertical starting phases. The peeler drives the vertical motion at $\nu_z = 1/2$ on the last several turns.

X. RESULTS

The half-width half-maximum amplitude of the vertical density experimentally found before entry into the extraction system is 23/32 in. The energy distribution of the external beam is insensitive to this amplitude since very few particles with amplitude larger than about 3/8 in. contribute to the external beam [see Fig. 21, $\eta(E,z)$]. The extraction efficiency, however, depends on z_{max} since this is a factor in the determination of the total number of particles started.

The total integrated extraction efficiency is given in Table 6 for several values of the maximum radial and vertical amplitudes and several distribution functions shown in Fig. 24.

Table 6. Calculated extraction efficiencies.

r_{max} (in.)	Vertical square wave z_{max}	Radial distribution			
		Uniform	Linear tail	Gaussian tail	Observed
3	5/8	6.06	10.2	11.4	12.7
	3/4	4.21	7.1	7.9	8.8
	7/8	3.1	5.2	5.8	6.5
6	5/8	2.87	5.57	6.70	8.20
	3/4	2.0	3.87	4.7	5.7
	7/8	1.47	2.84	3.4	4.2

The energy distribution of the external beam is shown in Fig. 25 for the observed vertical distribution of amplitude 23/32 in. (HWHM) and the observed radial distribution of 3 in. amplitude and an assumed amplitude of 6 in. (Fig. 14). The histogram is the experimentally determined energy distribution of the external beam of Friesen and Barkus.[25] The histogram

[25] S. Friesen and W. H. Barkas, Lawrence Radiation Laboratory Report, UCID-613 (1959).

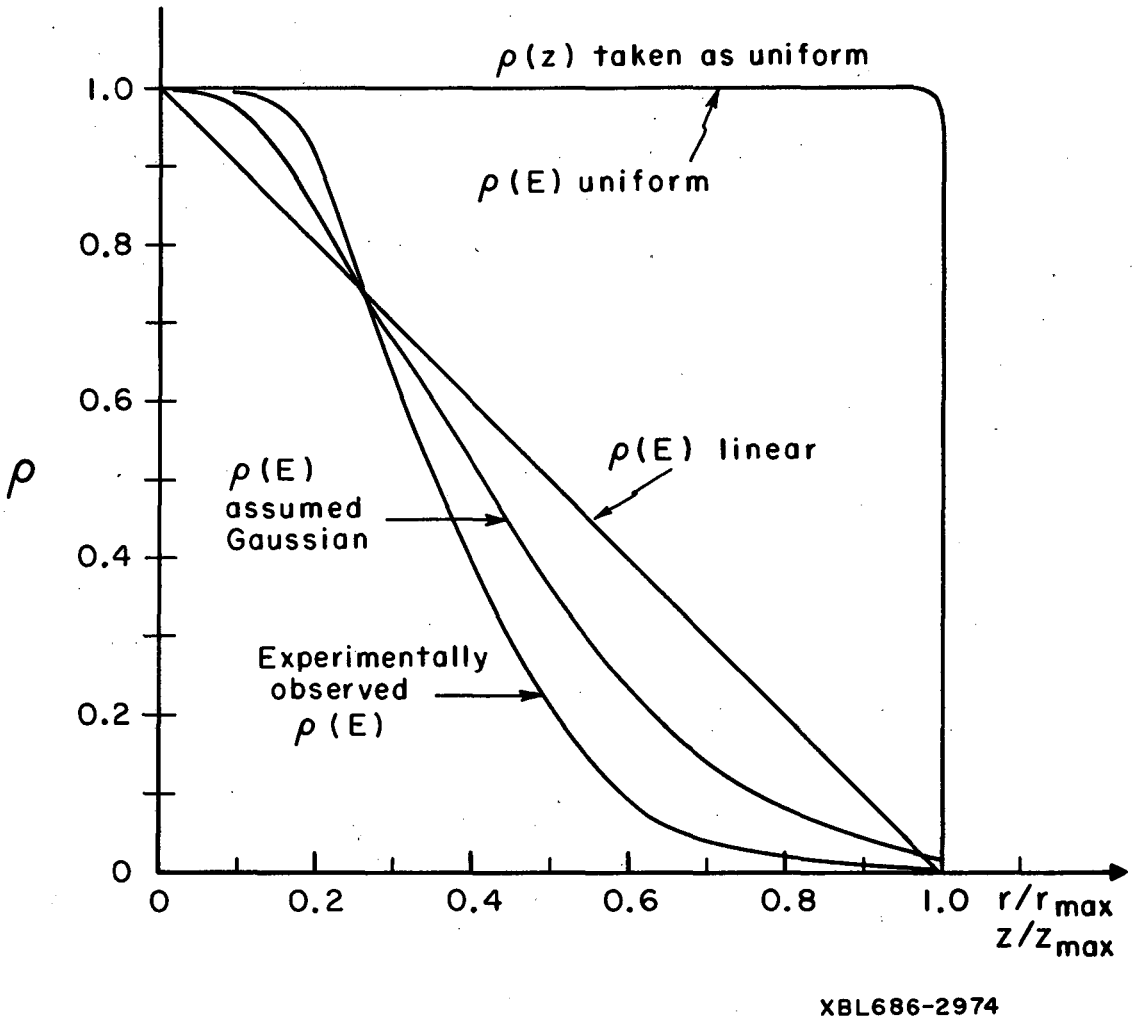

Fig. 24. Radial and vertical distributions used in Table 6.

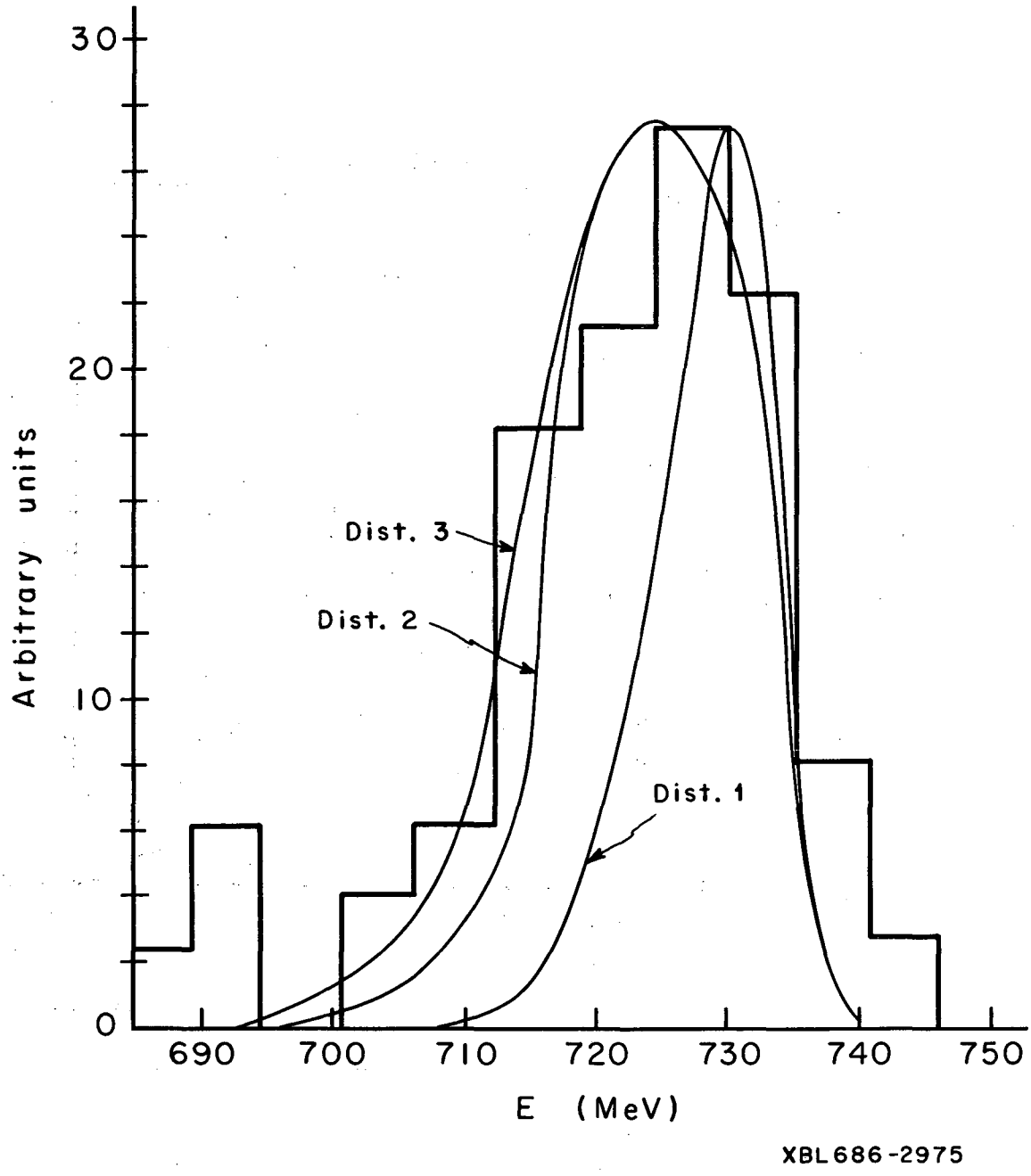

Fig. 25. Energy distribution of external beam. Histogram is measurement of Friesen and Barkas (UCID-613). Dist. 1 is based on measured radial and verticle particle distributions. Dist. 2 and Dist. 3 are attempted fits to Barkas' curve. See Fig. 14.

has been moved down 20 MeV in energy to account for the magnetic field difference between actual machine operation and the orbit calculations. The general shape of the distribution can easily be understood, Fig. 26. At high energy we have few particles in the radial phase space (small radial amplitude) but high extraction efficiency. As the energy is lowered, the number of particles increase, but the extraction efficiency decreases until at 690 MeV it is essentially zero.

Recently we performed a range energy measurement at the physics cave snout with a helium ion chamber and copper absorbers. The observed data is reasonably fit by a calculated curve for 746-MeV protons with a 10-MeV energy spread (5 MeV standard deviation). This energy spread is consistent with the observed 3-in. radial amplitude distribution (Fig. 25). Two physically separate beams emerge from the cyclotron. Both beams are of the same energy (746 MeV) and are of about equal intensity.

The relative extraction efficiency as a function of vertical amplitude was measured with the rotatable finger probe. The internal beam with vertical amplitude less than z_{finger} was monitored by counting the neutrons from an internal target. The regenerated beam reaching the physics cave snout was measured with a helium ion chamber and is plotted as normalized points in Fig. 27 as a function of vertical amplitude. The solid curve is the calculated extraction efficiency obtained by using the particle distribution inferred from the neutron yield of the target probe as a function of vertical amplitude. This distribution was noticeably different from the measured distribution obtained earlier. A calculated curve based on the vertical distribution of Fig. 11 is shown (dashed).

A computer-calculated beam spot is shown in Fig. 28. No vertical or horizontal restrictions have been imposed. Each × represents one or more particles and is located in the (y,R) physical space at 166 deg, 106 in. All particles have been successfully regenerated with the group on the right meeting the radial channel passage criteria. The group on the left will hit the channel septum bar. Figure 29 shows a beam spot photograph obtained at the physics cave snout. The division of the beam into two groups is evident. The two groups arrive at the same time and with the same energy and are of approximately the same intensity. The origin of this division is not understood.

XI. EFFECT OF LOW ENERGY PENETRATION INTO THE REGENERATOR

The extraction efficiency can be low if a significant portion of the beam entering the regenerator has a large radial oscillation amplitude. The radius at which regenerative extraction begins depends on the energy of the entering beam. Presently, rf acceleration of the beam continues throughout the entire extraction process, so a beam of large radial betatron oscillation amplitude enters the regenerator at correspondingly smaller energy. This low energy beam must penetrate deep into the vertically defocusing regenerator before extraction begins. During this period of deep penetration, the vertical amplitude can be increased sufficiently so as to incur vertical loss and drive other loss mechanisms. A beam of smaller radial betatron oscillation amplitude enters the regenerator later in time and, thus, at a higher energy. Such deep penetration

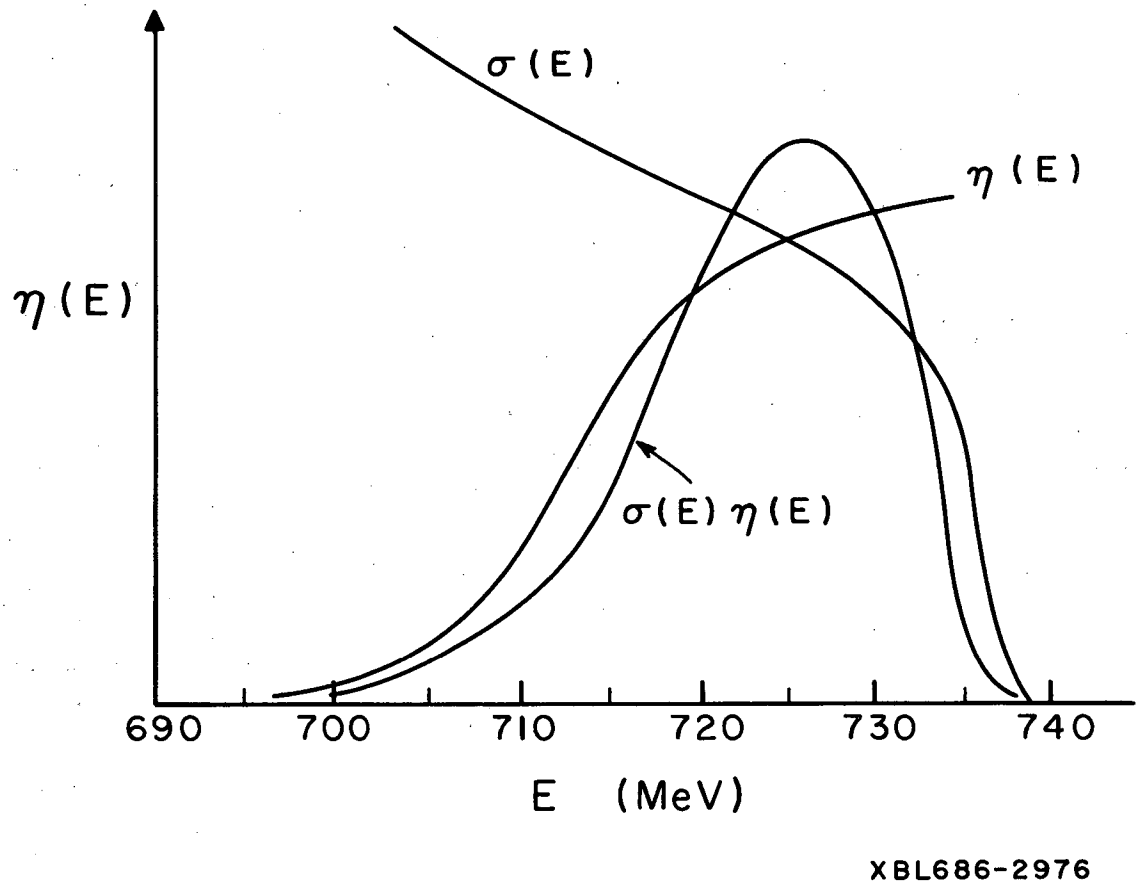

Fig. 26. Origin of the external beam spectrum shape.

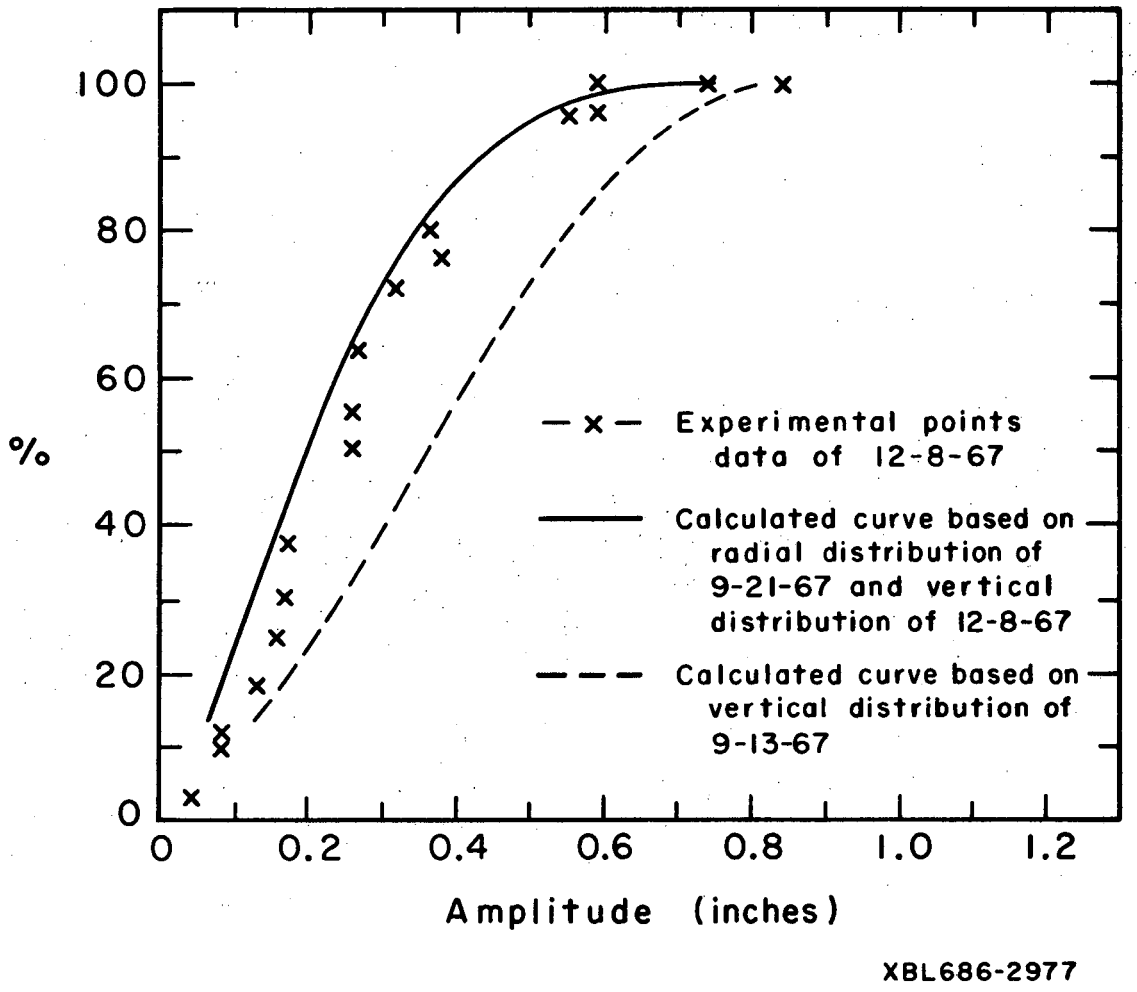

Fig. 27. Percent external beam (snout) as a function of vertical amplitude defined by finger probe.

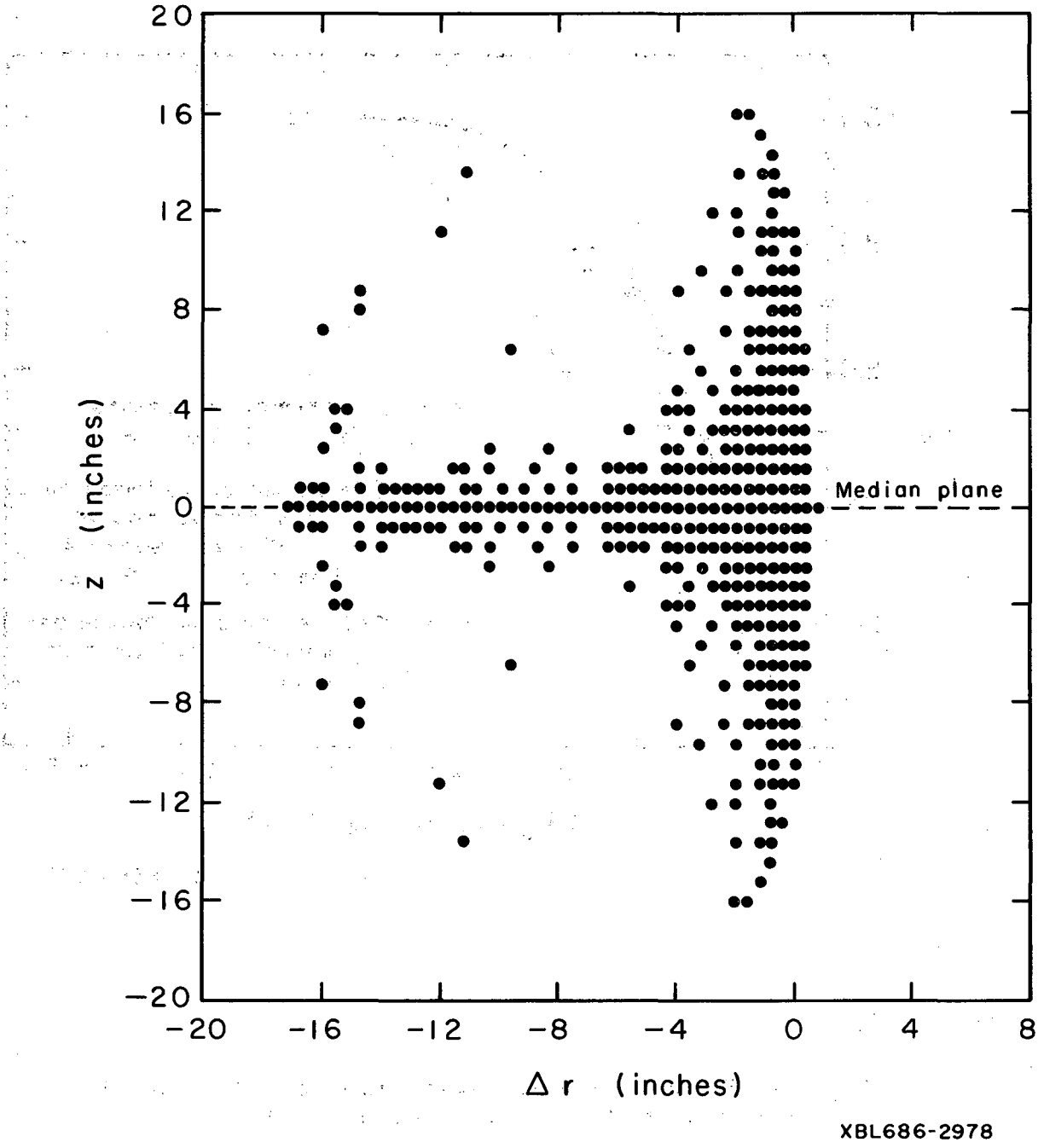

Fig. 28. Calculated beam spot at 106" 166° in the r, z plane with no radial or vertical aperture restrictions. Each (·) represents one or more particles.

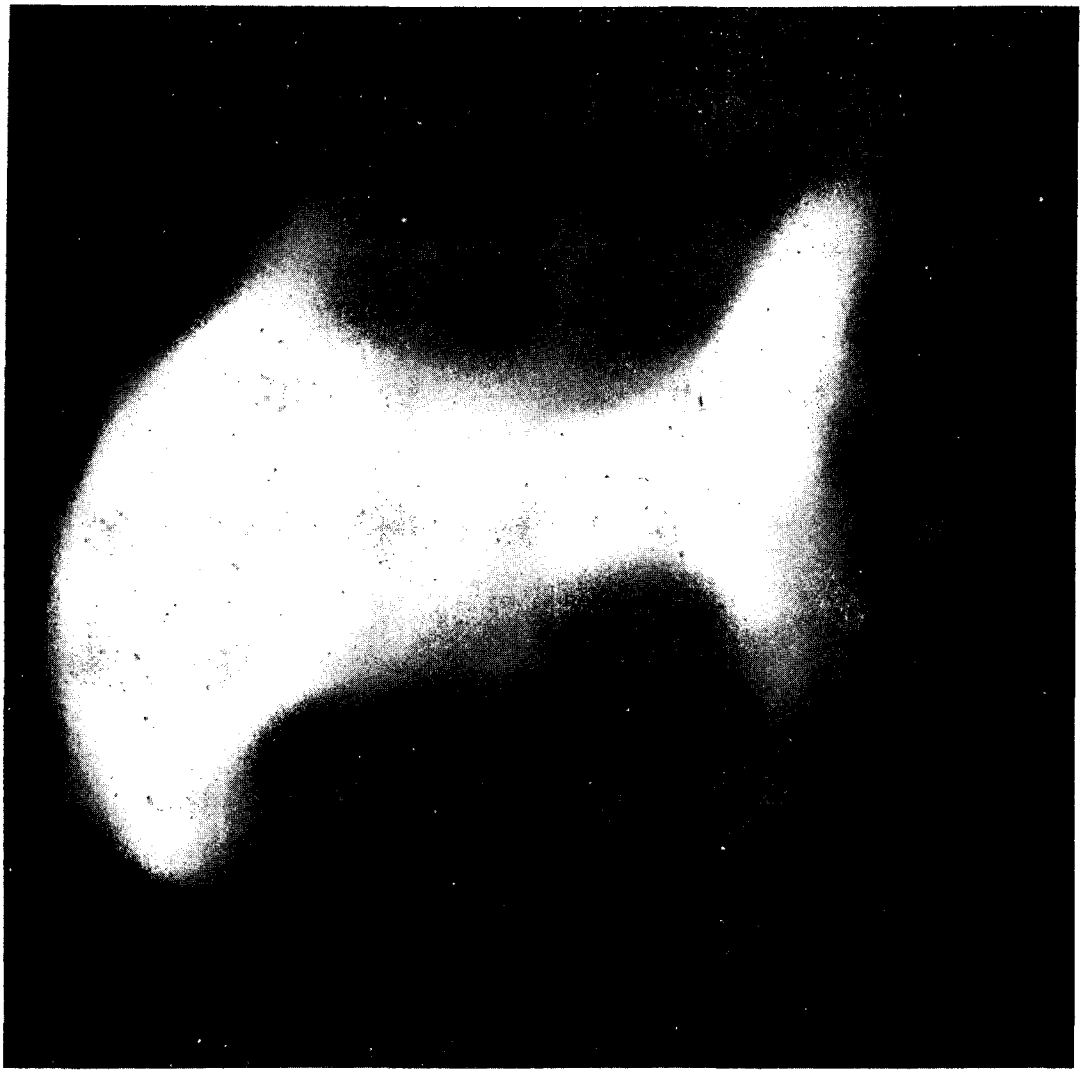

XBB 686-3660

Fig. 29. Beam spot at physics cave snout.

is not required for this higher energy beam in order for regenerative action to begin; no vertical loss occurs.

Coupling of the radial betatron oscillation amplitude to the vertical loss by premature penetration into the regenerator can be eliminated by the addition of a time-dependent magnetic perturbation to the existing magnetic field. The time dependence of this perturbation is determined by the beam pulse repetition frequency of the cyclotron. This magnetic perturbation would produce an off-centering of the orbits so that no particles enter the regenerator and so none are lost vertically. The rf acceleration is turned off. Extraction begins by reducing the magnetic field perturbation strength. The energy spread of all particles in the machine is then that associated with the synchronous phase oscillations and is independent of the radial betatron oscillation amplitude. This energy is sufficiently small so that a uniformly small penetration into the regenerator is required in order to initiate extraction at full energy, where no vertical loss occurs.

The importance of this Mode 1 loss as a function of energy was investigated by tracking unaccelerated orbits inside the stable region of the radial betatron phase space of the desired energy. Each orbit had sufficient regenerator penetration so as to make the same number of revolutions near the unstable fix point. The vertical amplitude growth during penetration into the regenerator is shown in Fig. 30. This vertical growth is sufficient at low energies so as to cause complete loss of the beam, Fig. 31. At higher energy the vertical amplitude is simply increased. Mode 2 and Mode 4 are sensitive to the vertical amplitude and hence Mode 1 drives these loss mechanisms. This is indicated by lines 12 and 14 of Fig. 1.

The following conclusions can be drawn for the measured phase space distributions scaled to a 6-in. maximum radial oscillation amplitude:

1. The extraction efficiency is 4-5%.

2. The energy distribution of the external beam agrees with that measured by Friesen and Barkas (22 MeV FWHM).[26]

3. Beam is lost vertically before the start of regeneration due to low energy penetration into the regenerator (Mode 1 loss). This loss accounts for something like 50% of the internal beam.

4. A time-varying magnetic perturbation will improve the extraction efficiency up to a maximum of 40% of the internal beam provided sufficient fringing field modifications are made to prevent crossing the Walkinshaw resonance and over focusing in the peeler.

---

[26] S. Friesen and W. H. Barkas, Lawrence Radiation Laboratory Report UCID-613 (1959).

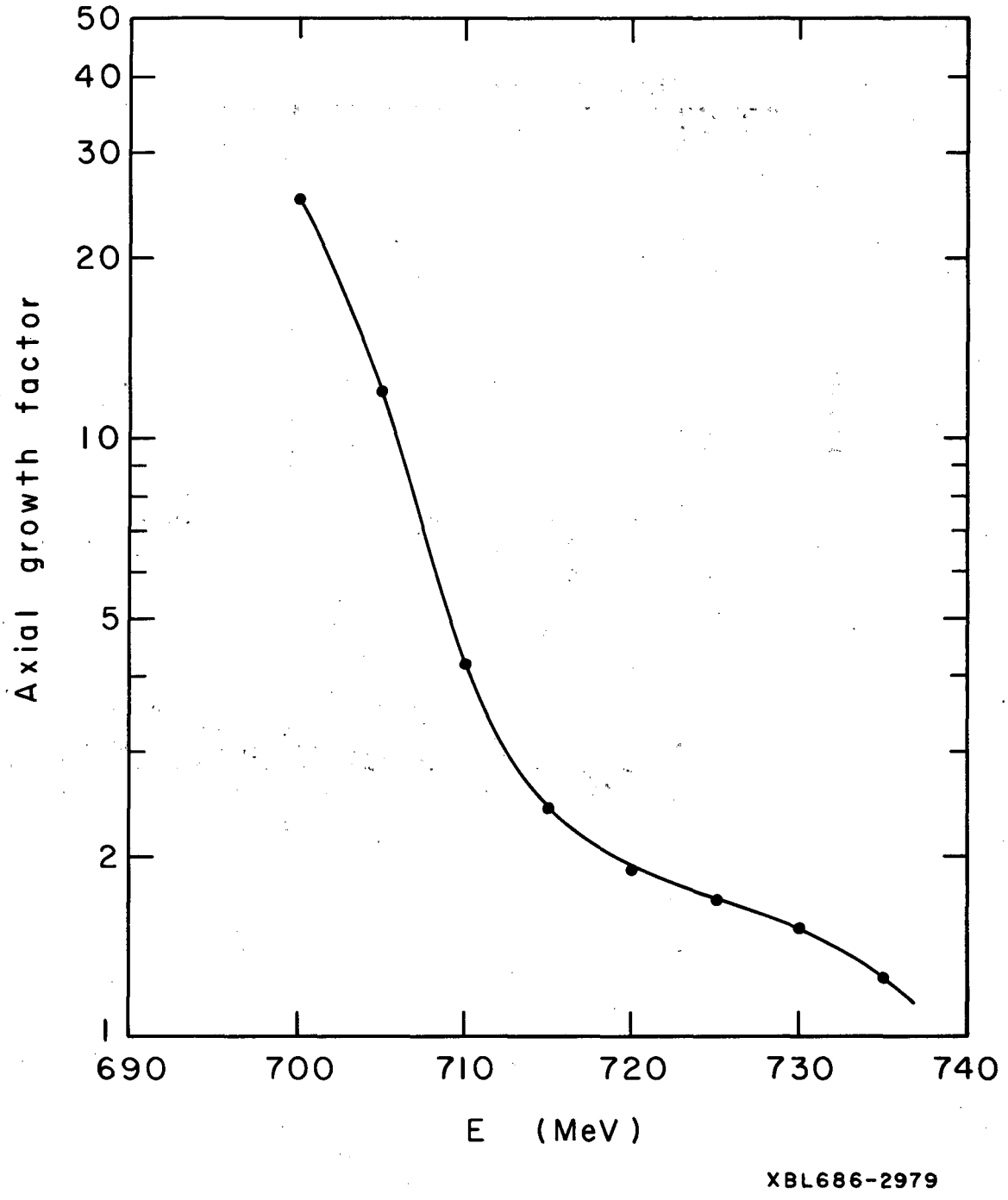

Fig. 30. Axial growth of beam due to Mode 1 (low energy penetration into regenerator).

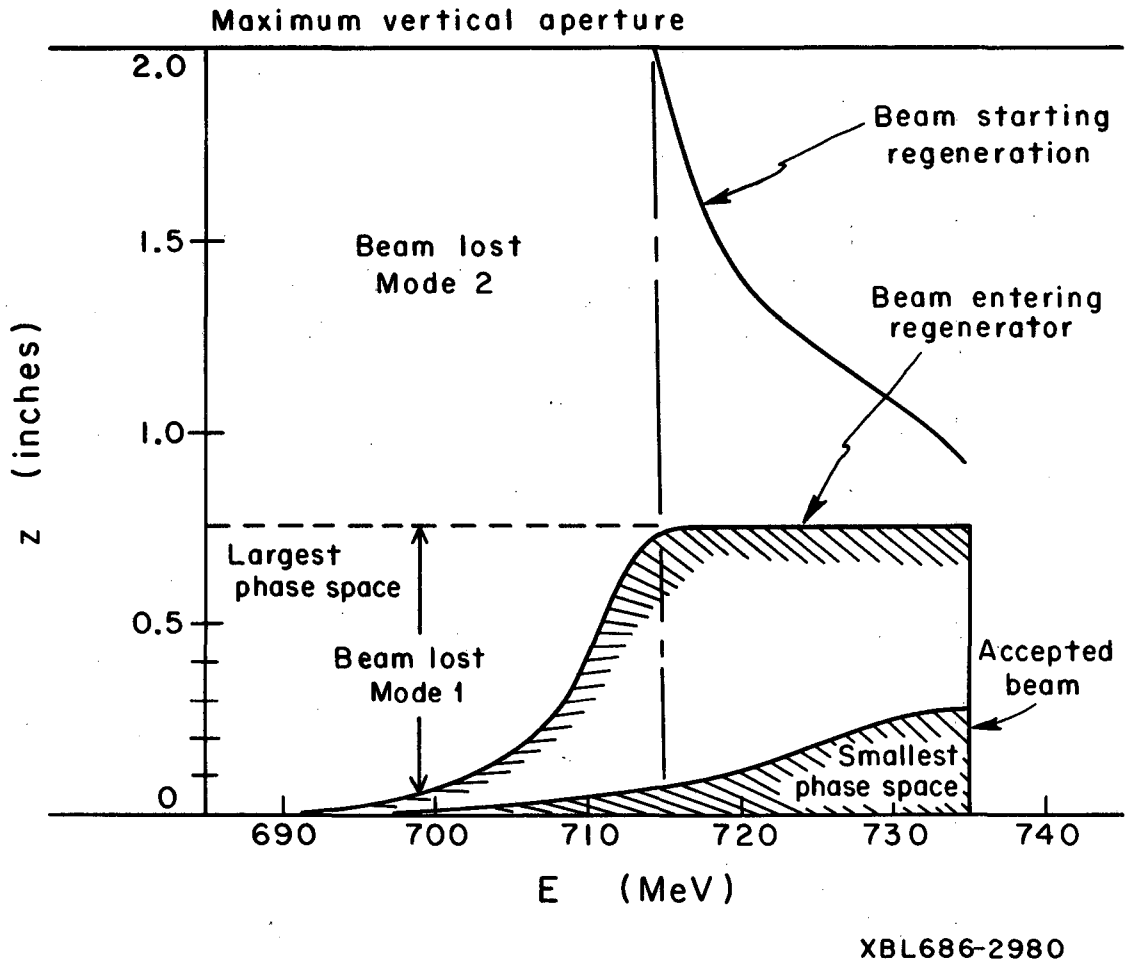

Fig. 31. Vertical loss vs energy for Mode 1.

However, when the measured maximum radial amplitude of 2-1/2 to 3 in. is used, the following conclusions are drawn:

1. The extraction efficiency is 9% for integration over the measured phase space distributions.

2. The energy distribution of the external beam is about half the width measured by Friesen and Barkas but agrees with the energy spread inferred from the measured Bragg peak.

3. No significant portion of the beam is lost from low energy penetration into the regenerator.